References

ABIMANYU, H., Jung, K.D., Jun, K.W., Kim, J., Yoo, K.S. 2008. Preparation and characterization of $Fe/Cu/Al_2O_3$ composite granules for SO_3 decomposition to assist hydrogen production. *Applied Catalysis A: General*:134-141.

ADAMS, T.A., Barton, P.I. 2009. A dynamic two-dimensional heterogeneous model for water gas shift reactors. *International Journal of Hydrogen Energy*, 34:887-8891.

AGNEW, J.B., Potter, O.E. 1970. Heat transfer properties of packed tubes of small diameter. *Trans. Instn. Chem. Engs.*, T15

AHMADI MOTLAGH, A.H., Hashemabadi, S.H. 2008. 3D CFD simulation and experimental validation of particle-to-fluid heat transfer in a randomly packed bed of cylindrical particles. *International Communications in Heat and Mass Transfer*, 35:1183-1189.

AHMADI MOTLAGH, A.H., Hashemabadi, S.H. 2008. CFD based evaluation of heat transfer coefficient from cylindrical particles. *International Communications in Heat and Mass Transfer*, 35:674-680.

AICHLMAYR, H.T., Kulacki, F.A. 2006. Effective conductivity of saturated porous media. *Advances in Heat Transfer*:377-460.

AICHLMAYR, H.T. & Kulacki, F.A. 2006. Effective conductivity of saturated porous media. *Advances in Heat Transfer*:377-460.

ANDREWS, J. & Shabani, B. 2012. Re-envisioning the role of hydrogen in a sustainable energy economy. International Journal of Hydrogen Energy, 37:1184-1203

ASSOCIATION, World Nuclear. 2010. www.world-nuclear.org/info.

ASTM STANDARD, D3908. 2008. *Standard test method for hydrogen chemisorption on supported platinum catalysts by volumetric vacuum method*. West Conshohocken.

BAHRAMI, M., Yovanovich, M.M., Culham, J.R. 2006. Effective thermal conductivity of rough spherical packed beds. *International Journal of Heat and Mass transfer*, 49:3691-3701.

BAI, H., Theuerkauf, J., Gillis, P.A. 2009. A coupled DEM and CFD simulation of flow field and pressure drop in fixed bed reactor with randomly packed catalyst particles. *Ind. Eng. Chem. Res.* , 48:4060-4074.

BAKER, M.J., Tabor, G.R. 2010. Computational analysis of transitional air flow through packed columns of spheres using the finite volume technique. *Computers and Chemical Engineering*, 34:878-885.

BAKER, M.J. 2011. *CFD simulation of flow through packed beds using the finite volume technique*. University of Exeter: PhD Thesis.

BALAKRISHNAN, A.R., Pei, D.C.T. 1979. Heat Transfer in gas-solid packed bed systems. 1. A critical review. *Ind. Eng. Chem. Process Des. Dev.*:30-40.

BANERJEE, A.M., Pai, M.R., Bhattacharya, K., Tripathi, A.K., Kamble, V.S., Bharadwaj, S.R., Kulshreshtha, S.K. 2008. Catalytic decomposition of sulfuric acid on mixed Cr/Fe oxide samples and its application in sulfur-iodine cycle for hydrogen production. *International Journal of Hydrogen Energy*:319-326.

BANERJEE, A.M., Pai, M.R., Meena, S.S., Tripathi, A.K., Bharadwaj, S.R. 2011. Catalytic activites of cobalt, nickel and copper ferrospinnels for sulfuric acid decompostion: The high temperature step in the sulfur based thermochemical water splitting cycles. *International Journal of Hydrogen Energy*: 36(8):4768-4780.

BARBAROSSA, V., Brutti, S., Diamanti, M., Sau, S., De Maria, G. 2006. Catalytic thermal decomposition of sulphuric acid in sulphur-iodine cycle for hydogen production. *International Journal of Hydrogen Energy*:883-890.

BAUER, R., Schlünder, E.U. 1978. Effective radial thermal conductivity of packings in gas flow. Part II. Thermal Conductivity of the packing fraction without gas flow. *International Chemical Engineering*, 18:189-204.

BAUER, R. 1990. Stagnant Packed Beds. Hemisphere Handbook of Heat Exchanger Design. Washington: Hemisphere Publishing Corporation. pp. 2.8. 1-1- 2.8.4-14.

BERTY, J.M. 1999. Experiments in catalytic reaction engineering. Fogelsville: Berty Reaction Engineers. 294 p.

BEUSCHLEIN, W.L. & Simenson, L.O. 1940. Solubulity of sulfur dioxide in water, 62:610-612.

BIRD, R. B ., Stewart, W.E., Lightfoot, E.N. 1960. Transport phenomena. New York: Wiley.

BORKAR, S.A., Dharwadkar, S.R. 2004. Temperatures and kinetics of anatase to rutile transformations in doped TiO_2 heated in micorwave field. *Journal of Thermal Analysis and Calorimetry*, 75:761-767.

BOSKOVIC, G., Dropka, N., Wolf, D., Bruckner, A., Bearns, M. 2004. Deactivation kinetics of Ag/Al_2O_3 catalysts for ethylene epoxidation. *Journal of Catalysis*, 226:334-342.

BOSSEL, U. 2006. Does a Hydrogen economy make sense? Proceeding of IEEE, October 2006, 94(10):1826-1837

BRECHER, L.E., Spewock, S., Warde, C.J. 1977. The Westinghouse sulphur cycle for the thermo-chemical decomposition of water. *International Journal of Hydrogen Energy*:7-15.

BRITTAIN, R.D. & Hildebrand, D.L. 1983. Catalytic decomposition of gaseous SO_3. *J. Phys. Chem.*:3713-3717.

BROWN, N.R., Revankar, S.T. 2012. A review of catalytic sulfur (VI) oxide decomposition experiments. *International Journal of Hydrogen Energy*, 37:2685-2698.

BRUTTI, S., De Maria, G., Cerri, G., Giovannelli, A., Brunetti, B., Cafarelli, P., Semprin, E., Barbarossa, V., Veroli, A. 2007. Decomposition of H_2SO_4 by direct solar radiation. *Ind. Eng. Chem. Res.*:6393-6400.

BURKE, S.P., Plummer, W.B. 1828. *Industrial Engineering Chemistry*, 20

CALIS, H.P.A., Nijerhuis, J., Paikert, B.C., Dautzenberg, F.M., van den Bleek, C.M. 2001. CFD modeling and experimental validation of pressure drop and flow profile in a novel structured catalytic reactor packing. *Chemical Engineering Science*, 56:1713-1720.

CARMAN, P.C. 1937. Fluid flow through a granular bed. *Trans. Inst. Chem. Eng. London*, 15:150-156.

CARTY, R.H., Mazumber, M.M., Schreider, J.K., Pangborn, J.B. 1981. *Thermochemical hydrogen production*. Chicago.

CASTILLO-ARAIZA, C.O., Jimenez-Islas, H., Lopez-Isunza, F. 2007. Heat-transfer studies in packed bed catalytic reactors of low tube/particle diameter ratio. *Ind. Eng. Chem. Res.*:7426-7435.

CAULKIN, R., Fairweather, M., Jia, X., Gopinathan, N., Williams, R.A. 2006. An investigation of packed columns using a digital packing algorithm. *Computers and Chemical Engineering*, 30:1178-1188.

CAULKIN, R., Ahmad, A., Fairweather, M., Jia, X., Williams, R.A. 2009. Digital predictions of complex cylinder packed columns. *Computers and Chemical Engineering*, 33:10-21.

CENGEL, Y.A., Ghajar, A.J. 2011. Heat and Mass Transfer: Fundamentals & Applications. McGraw-Hill. 802 p.

CHOI, Y.S., Kim, S.J., Kim, D. 2008. A semi-emperical correlation for pressure drop in packed beds of spherical particles. *Transp Porous Med.,* 75:133-149.

CHOI, J.H., Tak, N., Shin, Y.J., Kim, C.S., Lee, K.Y. 2009. Numerical analysis of a SO3 packed column decomposition with alloy RA330 structural material for nuclear hydrogen production using the Sulfur-Iodine process. *Nuclear Engineering and Technology*, 41(10):1275-1284.

COETZEE, M.D. 2008. *The chemical reactor for the decompostion of sulphuric acid for the hybrid sulphur process*. Potchefstroom. Ph.D. Thesis

COMSOL. 2013. *COMSOL Multiphysics Reference Manual*.

CONNOLLY, S.M., Zabolotny, E., McLaughlin, D.V., Lahoda, E.J. 2009. Design of a composite sulfuric acid decomposition reactor, concentrator and preheater for hydrogen production. *International Journal of Hydrogen Energy*, 34:4074-4087.

CORELLA, J., Asua, J.M. 1982. Kinetics of deactivation of a solid catalyst in a nonsimple reaction. Isobutene oxidation in gaseous phase by a parallel reaction network. *Ind. Eng. Chem. Process Des. Dev.*, 21:551-558.

DALMAN, M.T., Merkin, J.H., McGreavy, C. 1986. Fluid flow and heat transfer past two spheres in a cylindrical tube. *Computers and Fluids*, 14:267-281.

DE KLERK, A. 2003. Voidage variation in packed beds at small column to particle diameter ratio. *AIChE*, 49:2022-2029.

DELGADO, J.M.P.Q. 2006. A simple experimental technique to measure tortuosity in packed beds. *The Canadian Journal of Chemical Engineering*, 84:651-655.

DERKX, O.R., Dixon, A.G. 1996. Determination of the fixed bed wall heat transfer coefficient using computational fluid dynamics. *Numerical Heat Transfer Part A*, 29:777-794.

DIESSLER, R.G., Boegli, J.S. 1958. An investigation of effective thermal conductivities of powders in various gases. *ASME Transactions*, 80(7):1417-1425.

DINCER, I. 2012. Green methods for hydrogen production. *International Journal of Hydrogen Energy*, 37:1954-1971.

DIXON, A.G., Paterson, W.R., Cresswell, D.L. 1978. Heat transfer in packed beds of low tube/particle diameter ratio. *Chem. React. Eng. ACS Symp. Ser.*, 65:238.

DIXON, A.G., Cresswell, D.L. 1979. Theoretical prediction of effective heat transfer parameters in packed beds. *AIChE Journal*, 25:663.

DIXON, A.G., Nijemeisland, M. 2001. CFD as a design tool for fixed bed reactors. *Ind. Eng. Chem. Res.*, 40:5246-5254.

DIXON, A.G., Nijemeisland, M., Stitt, E.H. 2003. CFD simulation of reaction and heat transfer near the wall of a fixed bed. *International Journal of Chemical Reactor Engineering*, 1:A22.

DIXON, A.G., Taskin, M.E., Nijemeisland, M., Stitt, E.H. 2008. Wall-to-particle heat transfer in steam reformer tubes: CFD comparison of catalsyt particles. *Chemical Engineering Science*, 63:2219-2224.

DOKIYA, M., Kameyama, T., Fukuda, K, Kotera, Y. 1977. The study of thermochemical preparation. III. An oxygen evolving step through the thermal splitting of sulfuric acid. *Bulletin of the Chemical Society of Japan*:2657-2660.

DU TOIT, C.G. 2008. Radial variation in porosity in annular packed beds. *Nuclear Engineering and Design*:3073-3079.

ERGUN, S. 1952. Flow through packed columns. *Chem. Eng. Prog.*, 48

FAHIEN, R.W., Smith, J.M. 1955. Mass transfer in packed beds. *AIChE J.*, 1(28)

FILLA, M. 2003. Validation of a flux method for radiative heat transfer in plug flow reactors. (*In* 26th Combustion Meeting. Ishia.)

FOGLER, H.S. 2006. Elements of chemical reaction engineering. Saddle River: Pearson Education Inc. 1112 p.

FORZATTI, P., Lietti, L. 1999. Catalsyt Deactivation. *Catalysis Today*, 52:165-181.

FREUND, H., Zeiser, T., Huber, F., Klemm, E., Brenner, G., Durst, F., Emig, G. 2003. Numerical simulations of single phase reacting flows in randomly packed fixed-bed reactors and experimental validation. *Chemical Engineering and Science*, 58:903-910.

FROMENT, Gilbert F. & Kenneth B. Bischoff. 1979. Chemical Reactor Analysis and Design. John Wiley & Sons. p.

GEAGLA, A., Holte, J., Kapilow-Cohen, B., LaRiviere, M., Smith, C.L., Staub, J., Sweetnam, G., Wells, P. 2013. U.S. Energy Information Administration. http://www.eia.gov/

GELBARD, F., Andazola, J.S., Naranjo, G.E., Velasquez, C.E., Reay, A.R. 2005. *High pressure sulfuric acid decomposition experiments for the sulphur iodine thermo-chemical cycle*. Sandia National Laboratories. Report

GIACONIA, A., Sau, S., Felici, C., Tarquini, P., Karagiannakis, G., Pagkoura, C., Agraffiotis, C., Konstandopoulos, A.G., Thomey, D., de Oliveira, L., Roeb, M., Sattler, C. 2011. Hydrogen Production via sulfur-based thermochemical cycles: Part 2: Performance evaluation of Fe_2O_3 based catalysts for the sulfuric acid decomposition step. *International Journal of Hydrogen Energy*:6496-6509.

GINOSAR, D.M., Petkovic, L.M., Glenn, A.W., Burch, K.C. 2007. Stability of supported platinum sulfuric acid decomposition catalysts for use in thermochemical water splitting cycles. *International Journal of Hydrogen Energy*:482-488.

GINOSAR, D.M. 2009. *Catalysts: NHI Thermochemical Systems, FY 2009 Year End Report*. Idaho National Laboratories.

GINOSAR, D.M., Rollins, H.W., Petkovic, L.M., Burch, K.C., Rush, M.J. 2009. High-temperature sulfuric acid decomposition over complex metal oxide catalysts. *International Journal of Hydrogen Energy*:4065-4073.

GINOSAR, D.M., Petkovic, L.M., Burch, K.C. *Activity and stability of sulfuric acid decomposition catalysts for thermochemical water splitting cycles*. Idaho Falls.

GNIELINSKI, V. 1982. Berechnung des warme und stoffaustauschs durchstromten schuttungen. *Verfahrenstechnik*, 16:36.

GOVINDARAO, V.M.H. & Gopalakrishna, K.V. 1993. Solubility of sulfur dioxide at low partial pressures in dilute sulfuric acid solutions. *Ind. Eng. Chem. Res.*, 32:2111-2117.

GREGG, S.T., Sing, K.S.W. 1982. Adsorption, surface area & porosity. London: Academic Press.

GUARDO, A., Coussirat, M., Larrayoz, M.A., Recasens, F., Egusquiza, E. 2005. Influence of turbulence model in CFD modeling of wall-to-fluid heat transfer in packed beds. *Chemical Engineering Science*, 60:1733-1742.

GUNJAL, P.R., Ranade, V.V., Chaudhari, R.V. 2005. Computational study of a single-phase flow in packed bed of spheres. *American Institute of Chemical Engineers Journal*, 51:365-378.

HANDLEY, D., Heggs, P.J. 1968. Momentum and heat transfer in regularly shaped packing. *Trans. Inst. Chem. Eng.*, 46:251-264.

HAYDUK, W., Asatani, H., Lu, B.C.Y. 1988. Solubility of sulfur dioxide in aqueous sulfuric acid solutions. *J. Chem. Eng. Data*, 33:506-509.

HENNECKE, F.W., Schlünder, E.U. 1973. Warmeubergang in beheztein oder gekuhlten rohren mit schuttungen aus Kugeln, Zylindern un Rashig-ringen. *Chem. Ing. Techn.*, 45:277.

HSU, C.T., Cheng, P., Wong, K.W. 1994. Modified Zehner- Schlünder models for stagnant thermal conductivity of porous media. *International Journal of Heat and Mass transfer*, 37:2751-2759.

HUANG, C. & Raissi, A.T. 2005. Analysis of sulfur-iodine thermochemical cycle for solar hydrogen production. Part 1: decomposition of sulfuric acid. *Solar Energy*, 78:632-646.

IBERALL, A.S. 1950. Permeability of glass wool and other highly porous media. *Journal of Research of the National Bureau of Standards*, 45(5):398-406. November.

INCROPERA, F.P. & DeWitt, D.P. 2002. Fundamentals of heat and mass transfer. John Wiley & Sons, Inc. 981 p.

INDUSTRIES, EVONIK. 2007. *AEROXIDE TiO2 P25 - Hydrophilic Fumed Titanium Dioxide*. Hanua-Wolfgang.

IORDANIDIS, A.A. 2002. *Mathematical Modeling of Catalytic Fixed Bed Reactors*. Twente University Press. Ph.D. Thesis.

ISHIKAWA, H., Ishii, E., Uehara, I., Nakane, M. 1982. Catalyzed thermal decomposition of H_2SO_4 and production of HBr by the reaction of SO_2 with Br_2 and H_2O. *International Journal of Hydrogen Energy*, 7:237-246.

IVANOVA, E., Kovalev, V., Petrapavlovskii, A., Soroko, V, Forsov, A. 1991. Decomposition of sulfuric acid on a chromium phosphate catalyst. *Zh Prik Khim*, 64:257-261.

JAKOBSEN, H.A. 2011. *Fixed bed reactors - Lecture notes*.

JEFFERY, G.H., Bassett,J., Mendham, J., Denney, R.C. 1989. VOGEL's Textbook of quantitative chemical analysis. London: John Wiley and Sons Inc. 906 p.

KARAGIANNAKIS, G., Agraffiotis, C.C., Zygogianni, A., Pagkoura, C., Konstandopoulos, A.C. 2010. Hydrogen production via sulfur-based thermochemical cylces: Part 1: Synthesis and evaluation of metal oxide based candidate catalyst powders for sulfuric acid decomposition step. *International Journal of Hydrogen energy*, 36(4):2831-2844.

KARASAWA, H., Sasahira, A., Hoshino, K. 2005. Thermal Decomposition of SO_3. (*In* OECD/NEA Third Information Exchange Meeting of Nuclear Production of Hydrogen. Orai.)

KAVIANY, M. 1991. Principles of Heat Transfer in porous media. New York: Springer.

KIM, T., Gong, G.T., Lee, B.G., Lee, K.Y., Jeon, H.Y., Shin, C.H., Kim, H., Jung, K.D. 2006. Catalytic decompostion of sulfur trioxide on the binary metal oxide catalysts of Fe/Al and Fe/Ti. *Applied Catalysis A: General*:39-45.

KIM, J., Chang, J., Park, B.H., Shin, Y., Lee. K., Lee, W., Chang, J. 2008. A study on the dynamic behavior of sulfur trioxide decomposer for a nuclear hydrogen production. *International Journal of Hydrogen Energy*, 33:7361-7370.

KIM, C.S., Hong, S.D., Kim, Y.W., Kim, J.H., Lee, W.j., Chang, J. 2008. Thermal design of a laboratory-scale SO_3 decomposer for nuclear hydrogen production. *International Journal of Hydrogen Energy*, 33:3688-3699.

KOLB, G., Diver, R.B., Siegel, N., 2007. Central-station solar hydrogen power plant. Journal of Solar Energy Engineering, 129:179-183.

KONDAMUDI, K., Upadhyayula, S. 2012. Kinetic studies of sulfuric acid decomposition over Al-Fe_2O_3 catalyst in the sulfur Iodine cycle for hydrogen production. *International Journal of Hydrogen Energy*, 37(4):3586-3594.

KONING, G.W. 2002. *Heat and Mass Transport in Tubular Packed Bed Reactors at Reacting and non-Reacting Conditions*. Twente University Press. Ph.D. Thesis.

KUCHI, G., Ponyavin, V., Chen, Y., Sherman, S., Hechanova, A. 2008. Numerical modeling of high-temperature shell-and-tube heat exchanger and chemical decomposer for hydrogen production. *International Journal of Hydrogen Energy*, 33(20):5460-5468.

KUNII, D., Smith, J.M. 1960. Heat transfer characteristics of porous rocks. *AIChE Journal*, 6(1):71-78.

LEE, Y.H., Lee, J.I., No, H.C. 2010. A point model for the design of a sulfur trioxide decomposer. *International Journal of Hydrogen Energy*:5210-5219.

LEMCOFF, N.O., Pereira Duarte, S.I., Martinez, O.M. 1990. Heat Transfer in Packed Beds. *Reviews in Chem.l Eng.*:229.

LEVA, M. 1959. Fluidisation. New York: McGraw-Hill Book Company.

LEVENSPIEL, O. 1999. Chemical Reaction Engineering. John Wiley & Sons. 578 p.

LI, C-H., Finlayson, B.A. 1977. Heat transfer in packed beds- a reevaluation. *Chem. Eng. Sci.*, 32:1055.

LIF, Johan., Skoglundh, M., Lowendahl, L. 2002. Sintering of nickel particles supported on alumina in ammonia. *Applied Catalysis A: General*, 228:145-154.

LIN, S.S. & Flaherty, R. 1983. Design studies of the sulfur trioxide decomposition reactor for the sulfur cycle hydrogen production process. *International Journal of Hydrogen Energy*, 8(8):589-596.

LOGTENBERG, S.A., Dixon, A.G. 1998. Computational fluid dynamics studies of fixed bed heat transfer. *Chemical Engineering and Processing*, 37:7-21.

LOGTENBERG, S.A., Nijemeisland, M., Dixon, A.G. 1999. Computational fluid dynamics simulations of fluid flow and heat transfer at wall-particle contact points in a fixed bed reactor. *Chemical Engineering Science*, 54:2433-2439.

MACDONALD, T.F., El-Sayer, M.S., Mow, K., Dullen, F.A.L. 1979. Flow through proous media: The Ergun equation revisited. *Industrial and Engineering Chemistry Fundamentals*, 18:199-208.

MARTIN, H., Nilles, M. 1993. Radiale warmeleitung in durchstromten schuttungsrohren. *Chem. Ing. Techn.*, 65:1468.

MAYNARD, R.K. 2011. *Total hemispherical emissivity of very high temperature reactor (VHTR) candidate materials: Haslloy X, Haynes 230 and Alloy 617*. Ph.D. Thesis

MEARS, D.E. 1971. *Ind. Eng. Chem. Process Des. Develop.*, 10(4)

MEARS, D.E. 1976. *Ind. Eng. Chem. Fundam.*, 15(1)

MEULLER, G.E. 2005. Numerical packing spheres in cylinders. *Powder Technology*, 159:105-110.

MILES, F.D. & Fenton, J. 1919. The solubility of sulphur dioxide in sulphuric acid.

MILES, F.D. & Carson, T. 1946. The solubility of sulphur dioxide in fuming sulphuric acid.

MIRHASHEMI, F.S., Hashemabadi, S.H., Noroozi, S. 2011. CFD simulation and experimental validation for wall effects on heat transfer of finite cylindrical catalyst. *International Communications in Heat and Mass Transfer*, 38:1148-1155.

MIRHASHEMI, F.S., Hashemabadi, S.H. 2012. Experimental and CFD study of wall effects on orderly stacked cylindrical particles heat transfer in a tube channel. *International Communications in Heat and Mass Transfer*, 39:449-455.

MONZON, A., Garetto, T.F., Borgna, A. 2003. Sintering and redispersion of Pt/Al_2O_3 catalysts: a kinetic model. *Applied Catalysis A: General*, 248:279-289.

MORGAN, T. 2006. The hydrogen economy. United Nations Environment Programme. Non-technical Review. 44 p.

NAGARAJA, B.M., Jung, K.W., Ahn, B.S., Abimanyu, H., Yoo, K.S. 2009. Catalytic decomposition of SO_3 over $Pt/BaSO_4$ materials in sulfur-iodine cycle for hydrogen production. *Ind. Eng. Chem. Res.*:1451-1457.

NAGARAJAN, V., Ponyavin, V., Chen, Y., Vernon, M.E., Pickard, P., Hechanova, A.E. 2009. CFD modelling and experimental validation of sulphur trioxide decomposition in bayonet type heat exchanger and

chemical decomposer for different packed bed designs. *International Journal of Hydrogen Energy*, 34:2543-2557.

NAKAJIMA, H., Sakurai, M., Ikenoya, K., Hwang, G.J., Onuki, K., Shimizu, S. 1999. A study on a closed-cycle hydrogen production by thermochemical water-splitting IS process. 7th International Conference on Nuclear Engineering, Tokyo, Japan, April 19-23. ICONE-7104.

NANDAKUMAR, K., Shu, Y., Chuang, K.T. 1999. Predicting geometrical properties of random packed beds from computer simulation. *AIChE Journal*, 45(11):2286-2297.

NIELD, D.A. & Bejan, A. 2006. Convection in Porous Media. New York: Springer Science + Bussiness Media Inc. 654 p.

NIJEMEISLAND, M., Dixon, A.G. 2001. Comparison of CFD simulations to experiment for convective heat transfer in gas-solid fixed bed. *Chemical Engineering Journal*, 82:231-246.

NIJEMEISLAND, M., Dixon, A.G., Stitt, E.H. 2004. Catalyst design by CFD for heat transfer and reaction in steam reforming. *Chemical Engineering Science*, 59:5185-5191.

NOGLIK, A., Roeb, M., Sattler, C., Pitz-Paal, R. 2010. Modeling of a solar reciever-reactor for sulfur-based thermochemical cycles for hydrogen generation. *International Journal of Energy Research*

NOLAN, G.T., Kavanagh, P.E. 1995. Random packing of non-spherical particles. *Powder Technology*, 84:199-205.

OHNO, T., Sarukawa, K., Tokieda, K., Matsumura, M. 2001. Morphology of a TiO2 photocatalyst (Degussa, P-25) consisting of anatase and rutile crystaline phases. *Journal of Catalysis*, 203:82-86.

OKAZAKI, M., Ito, I., Toei, R. 1977. Effective thermal conductivities of wet granular materials. *AIChE Symposium Series*, 163:164-176.

OLBRICH, W.E., Potter, O.E. 1972. Heat transfer in small-diameter packed beds. *Chem. Eng. Sci.*, 27

OZTRUK, I.T., Hammache, A., Bilgen, E. 1995. An improved process for $H2_SO_4$ decomposition step of the sulphur-iodine cycle. *Energy Convers. Mgmt*, 36(1):11-21.

PARK, J., Cho, J.H., Jung, H., Jung, K.D., Kumar, S., Moon, I. 2013. Simulation and experimental study on the sulfuric acid decomposition process of SI cycle for hydrogen production. *International Journal of Hydrogen Energy*, 38:5507-5516.

PARSONS, I.M., Porter, K.E. 1992. Gas flow patterns in packed beds: A computational fluid dynamics model for wholly packed domains. *Gas Separation and Purification*, 6:221-227.

PEI, A.R. Balakrishnan & D.C.T. 1974. Heat transfer in fixed beds. *Ind. Eng. Chem. Process. Develop*

PETKOVIC, L.M., Ginosar, D.M., Burch, K.C. 2007. Titania-supported platinum group metal catalysts for sulfur based thermochemical water splitting cycles. (*In* AIChE Annual Meeting. Salt Lake City.)

PETROPAVLOVSKII, A., Kovalev, V., Soroko, V., Forsov, A. 1989. Kinetics of decomposition of sulfuric acid on an alumina-palladium catalyst. *Zr Prik Khim*, 62:2183-2185.

POLLET, B.G. 2013. Mission and objectives of the Hydrogen South Africa (HySA) Systems Competence Centre. Fuel Cells Bulletin, 2013(10): 10-17.

PREC. 2014. Professorship of renewable energy carriers. ETH Zurich, Department of mechanical and process engineering. http://www.pre.ethz.ch/

RAMALLO-LOPEZ, J.M., Requejo, F.G., Craievech, A.F., Wei, J., Avalos-Borja, M., Iglesia, E. 2005. Complementary methods for cluster size distribution measurements: suported platinum nanoclusters in methane reforming catalysts. *Journal of Molecular Catalysis A: Chemical*, 228:299-307.

RASHKEEV, S.N., Ginosar, D.M., Petkovic, L.M., Farrell, H.H. 2009. Catalytic activity of supported metal particles for sulfuric acid decomposition. *Catalsyis Today*, 139:291-298.

REXWINKEL, G., Heesink, A.B.M., van Swaaij, W.P.M. 1997. Mass transfer in packed beds at low Peclet numbers-wrong experiments or wrong interpretations? *Chem. Eng. Sci.*, 52:3995.

ROBERTS, S. 2012. *Personal Correspondence*. University of Cape Town - Catalysis Research Centre. Stephen.roberts@uct.ac.za

ROBOLD, K. 1982. *Warmetransport im inneren und in der randzone von Kugelschuttungen*. Julich.

RODRIGUEZ, G., Robin, J.C., Billot, P., Berjon, A., Cachon, L., Carles, P., Leybros, J., Le Naour, F., Pra, F., Terlain, A., Tochon, P. 2006. Development of a key component of the Iodine Sulfur thermochemical cycle: the SO_3 decomposer. (*In* WHEC 16. Lyon, France. p. 1-8.)

ROMKES, S.J.P., Dautzenberg, F.M., van den Bleek, C.M., Calis, H.P.A. 2003. CFD modeling and experimental validation of particle-to-fluid mass and heat transfer in packed bed at very low channel to particle diamter ratio. *Chemical Engineering Journal*, 96:3-13.

SALVAT, W.I., Mariani, N.J., Barreto, G.F., Martinez, O.M. 2005. An algorithm to simulate packing structure in cylindrical containers. *Catalysis Today*, 107-108:513-519.

SHERWOOD, T.K. 1925. Solubilities of sulfur dioxide and ammonia in water. *Industrial and Engineering Chemistry*, 17:745-747.

SHIN, Y., Chang, J., Kim, J., Park, B., Lee, K., Lee, W., Chang, J. 2009. A dynamic simulation of the sulfuric acid decomposition process in a Sulfur-Iodine nuclear hydrogen production plant. *Nuclear Engineering and Technology*, 41(6):831-840.

SLAVIN, A.J., Arcas, V., Greenhalgh, C.A., Irvine, E.R., Marshall, D.B. 2002. Theoretical model for the thermal conductivity of a packed bed of solid spheroids in the presence of a static gas, with no adjustable parameters except at low pressure and temperature. *International Journal of Heat and Mass Transfer*:4151-4161.

SMITH, J.M., Van Ness, H.C., Abbott, M.M. 2001. Introduction to chemical engineering thermodynamics. New York: McGraw-Hill. 817 p.

SPECCHIA, V., Baldi, G., Sicardi, S. 1980. Heat transfer in packed bed reactors with one phase flow. *Chem. Eng. Comm.*, 4:361.

SPEWOCK, S., Brecher, L.E., Talko, F. 1976. The thermal catalytic decomposition of sulfur trioxide to sulfur dioxide and oxygen. (Coral Gables: University of Miami Press.)

STEWART, W.E., Marr, D.F., Nam, T.T., Gola-Galimidi, A.M. 1991. Transport modeling of packed-tube reactors-1. Framework for a data-based approach. *Chemical Engineering Science*, 46:2905-2911.

SUMMERS, W.A., Steimke, J.L. 2005. Development of the hybrid sulphur thermo-chemical cycle. (*In* Nuclear Production of Hydrogen: Third information Exhange meeting. Oarai, Japan: OECD. p. 413.)

SUMMERS, W.A., Gorensek, M.B., Buckner, M.R. 2005. The hybrid sulphur cycle for nuclear hydrogen production. (*In* Global 2005. Tsukuba, Japan. p. 1-6.)

SUMMERS, W.A. 2012. SO_2 electrolysis and the Hybrid Sulfur process for hydrogen production. (*In* Hydrogen production and water electrolysis short course. Potchefstroom. p. 210-235.)

SUMMERS, A.W. & Steimke, J.L. 2005. Development of the hybrid sulfur thermochemical cycle. (*In* Nuclear Production of Hydrogen: Third Information Exchange Meeting. Oarai, Japan 5-7 October: OECD Publishing. p. 413.)

TASKIN, M.E. 2007. *CFD simulation of transport and reaction in cylindrical catalyst particles*. Worcester Polytechnic Institute: PhD Thesis.

THOENES, D., Kramers, H. 1958. Mass transfer from spheres in various regular packings to a flowing fluid. *Chem. Eng. Sc.*, 6:271.

THOMEY, D., de Oliveira, L., Sack, J.P., Roeb, M., Sattler, C. 2012. Development and test of a solar reactor for decomposition of sulphuric acid in thermochemical hydrogen production. *International Journal of Hydrogen Energy*, 37:16615-16622.

TOWNSEND, T.M., Allanic, A., Noonan, C., Sodeau, J.R. 2012. Characterization of sulfurous acid, sulfite and bisulfite aerosol systems. *The Journal of Physical Chemistry*, 116:4035-4046.

TSOTSAS, E. 2002. Hemisphere handbook of heat exchanger design. Washington: Hemisphere Publishing Corporation.

VAN ANTWERPEN, W. 2009. *Modeling the effective thermal conductivity in the near wall region of a packed pebble bed*. Potchefstroom: PhD Thesis.

VAN ANTWERPEN, W., Rousseau, P.G. 2009. Multi-Sphere unit cell model to calculate the effective thermal conductivity in pebble beds of mono sizedd spheres. *Nuclear Engineering and Design*: 183-201

VOTRUBA, J., Hlavacek, J., Marek, M. 1972. Packed bed axial thermal conductivity. *Chem. Eng. Sci.*, 27:1845.

WELTY, J.R., Wicks, C.E., Wilson, R.E., Rorrer, G.L. 2008. Fundamentals of momentum, heat and mass transfer. John Wiley & Sons, Inc. 711 p.

WESTERTERP, K.R., van Swaaij, W.P.M., Beenackers, A.A.C.M. 1984. Chemical reactor design and operation. John Wiley & Sons. p.

WILHELM, E., Battino, R., Wilcock, R.J. 1977. Low-pressure solubility of gases in liquid water. *Chemical Reviews*, 70(2):219-262.

XANH, Lá. 2005. Hydrogen and fuel cell. http://nl-hydrogen.blogspot.com/2005/02/h2-fuel-of-future.html Date of access: 27 April 2012.

YAGI, S., Kunii, D. 1957. Studies on effective thermal conductivities in packed beds. *AIChE Journal*, 3:373-377.

YAGI, S., Kunii, D. 1961. Fluidized-solids reactors with continuous solid feed-I:Residence time of particles in fluidized beds. *Chemical Engineering Science*, 16:364-371.

YAWS, C.L. 1999. Chemical Properties Handbook. McGraw-Hill. 779 p.

ZDRAVKOV, B.D., Cermak, J.J., Sefara, M., Janku, J. 2007. Pore classification in the characterization of porous materials: A perspective. *Central European Journal of Chemistry*, 5(2):385-395.

ZEHNER, P., Schlünder, E.U. 1970. Warmeleitfahigkeit von schuttugen bei mabigen temperaturen. *Chemie-Ing.-Techn.*, 42:933-941.

ZHANG, Q., Wang, H., Dalla Lana, I.G., Chuang, K.T. 1998. Solubility of sulfur dioxide in sulfuric acid of high concentration. *Ind. Eng. Chem. Res.*, 37:1167-1172.

ZHOU, R.P., Yu, A.B. 1995. The packing of spheres in a cylindrical container: The thickness effect. *Chemical Engineering Science*:1504-1507.

A. Appendix A: Transport Properties Correlations

A1: Pressure Drop

Friction factors from various scientists with their applicability range in terms of Reynolds number:

	Name	Equation	Reynolds Range
1	**Ergun Equation**	$f = \frac{1-\varepsilon}{\varepsilon^3}\left(1.75 + 150\frac{1-\varepsilon}{\mathrm{Re'}}\right)$	$\mathrm{Re}/(1-\varepsilon) < 500$
2	**Handley & Heggs**	$f = \frac{1-\varepsilon}{\varepsilon^3}\left(1.24 + 368\frac{1-\varepsilon}{\mathrm{Re'}}\right)$	$1000 < \mathrm{Re}/(1-\varepsilon) < 5000$
3	**Hicks**	$f = 6.8\frac{(1-\varepsilon)^{1.2}}{\varepsilon^3}\mathrm{Re}^{-0.2}$	
4	**Leva**	$\frac{dp_t}{dz} + 200G\frac{\mu(1-\varepsilon)^2}{d_p^2\psi^2\rho_g g\varepsilon^3} = 0$ $\frac{dp_t}{dz} + 3.5\frac{G^{1.9}\mu^{0.1}(1-\varepsilon)^{1.1}}{d_p^{1.1}\psi^{1.1}\rho_g g\varepsilon^3} = 0$	Laminar Turbulent
5	**Leva**	$\frac{dp_t}{dz} + \frac{2f_m G^2(1-\varepsilon)^{3-n}}{d_p\psi^{3-n}\rho_g g\varepsilon^3} = 0$	Laminar and Turbulent

Carman-Kozeny Permeability (Baker, 2011):

$$K_{pb} = \frac{\varepsilon^3}{180(1-\varepsilon)^2}d_p^2 \qquad [64]$$

A1.2 Particle Reynolds number (Baker, 2011)***:***

$$\mathrm{Re}_{d_p} = \frac{u\rho d_p}{\mu(1-\varepsilon)} \quad [65]$$

A1.3 Particle Volume equivalent diameter (Baker, 2011)***:***

$$d_p = \frac{6(1-\varepsilon)}{a_p} \quad [66]$$

Where:

- a_p is the specific surface area, $\frac{S_p}{V_p}$
- S_p is the particle surface area
- V_p is the particle volume

A2: Heat Transfer Correlations

A2.1: Thermal conductivity in packed bed

Levas correlation (Brecher, 1977)

$$\frac{\alpha_i d_t}{\lambda_g} = 0.813\left(\frac{d_p G}{\mu}\right)^{0.9} e^{-6d_p/d_t} \quad [67]$$

A2.2: Radial Effective thermal conductivity

A2.2.1 Bauer & Schlünder (Bauer, 1978)

$$\frac{\lambda_{convection}}{\lambda_f} = \frac{\rho u c_p}{\lambda_f} \frac{X_F}{8\left[2-\left(1-2\,d_{pv}/d_t\right)^2\right]} \quad [68]$$

$X_F = Fd_{pv}$ with F=1.75 for cylindrical particles

$$\frac{\lambda_{conduction,radiation}}{\lambda_f} = \left(1-\sqrt{1-\varepsilon}\right)\left(1+\varepsilon\frac{\lambda_{radiation}}{\lambda_f}\right)+\sqrt{1-\varepsilon}\left(\frac{\lambda_{rs}}{\lambda_f}\right)$$

$$\frac{\lambda_{radiation}}{\lambda_f} = 2.27\cdot 10^{-7}\,\frac{e}{2-e}T^3\frac{d_{pv}}{\lambda_f}$$

$$\frac{\lambda_{rs}}{\lambda_f} = \frac{2}{N}\left[\frac{B\left(k_s+k_r-1\right)}{N^2 k_s}\ln\left(\frac{k_s+k_r}{B}\right)+\frac{B+1}{2B}\left(k_r-B\right)-\frac{B-1}{N}\right]$$

$$N = \frac{k_s+k_r-B}{k_s}$$

$$B = C\left(\frac{1-\varepsilon}{\varepsilon}\right)^{10/9}$$

$$k_s = \frac{\lambda_{solid}}{\lambda_f}$$

$$k_r = \frac{\lambda_{radiation}}{\lambda_f}$$

X_F is effective mixing length, $X_F = Fd_{pv}$

F=1.75 for cylindrical particles

C=2.5 for cylindrical particles

A2.2.2 Dixon (Dixon, 1979)

$$\frac{1}{Pe_{er}} = \frac{1}{Pe_{fr}}+\frac{\lambda_{rs}/\lambda_f}{\mathrm{Re}\,\mathrm{Pr}}\left[\frac{Bi_f+4}{Bi_f}\right]\left[\frac{8}{N_s}+\frac{Bi_s+4}{Bi_s}\right]^{-1} \qquad [69]$$

(Re>50)

$$\frac{1}{Pe_{er}} = \frac{1}{Pe_{fr}}\left[\frac{Bi_s+4}{Bi_s}\right]\left[\frac{8}{N_F}+\frac{Bi_f+4}{Bi_f}\right]^{-1}+\frac{\lambda_{rs}/\lambda_f}{\mathrm{Re}\,\mathrm{Pr}} \qquad \text{(Re<50)}$$

$$\frac{1}{Pe_{rf}} = \frac{1}{Pe_{rf}(\infty)} + \frac{0.74\varepsilon}{\mathrm{Re}\,\mathrm{Pr}}$$

$Pe_{rf}(\infty) = 7$ for cylindrical particles

$$\frac{\lambda_{rs}}{\lambda_f} = \sqrt{1-\varepsilon}\,\frac{2}{M}\left[\frac{B(k_s-1)}{M^2 k_s}\ln\left(\frac{k_s}{B}\right) - \frac{B+1}{2} - \frac{B-1}{M}\right]$$

$$M = \frac{k_s - B}{k_s} \qquad k_s = \frac{\lambda_{solid}}{\lambda_f} \qquad B = C\left(\frac{1-\varepsilon}{\varepsilon}\right)^{10/9}$$

$$Bi_f = Nu_{wf}\left(d_t/2d_{pv}\right)\left(Pe_{rf}/(\mathrm{Re}\,\mathrm{Pr})\right) \qquad Nu_{fs} = 2.0 + 1.1\mathrm{Pr}^{1/3}\,\mathrm{Re}^{0.6}$$

$$Nu_{wf} = 0.523\left(1-d_{pv}/d_t\right)\mathrm{Pr}^{0.33}\,\mathrm{Re}^{0.738} \qquad Bi_s = 0.48 + 0.192\left(d_t/d_{pv}-1\right)^2 \text{ for cylinders}$$

$$\beta_s = \frac{\lambda_{rs}/\lambda_f}{\frac{8}{N_s} + \frac{Bi_s+4}{Bi_s}} \qquad \beta_f = \frac{\mathrm{Re}\,\mathrm{Pr}/Pe_{rf}}{\frac{8}{N_s} + \frac{Bi_f+4}{Bi_f}} \qquad N_s = \frac{0.25(1-\varepsilon)\frac{A_p}{V_p}\frac{d_t^2}{d_{pv}}}{\frac{\lambda_{rs}}{\lambda_f}\left[\frac{1}{Nu_{fs}} + \frac{1}{\beta}\frac{\lambda_f}{\lambda_{solid}}\right]}$$

$$N_F = \frac{0.25(1-\varepsilon)\frac{A_p}{V_p}\frac{d_t^2}{d_{pv}}}{\frac{\mathrm{Re}\,\mathrm{Pr}}{Pe_{rf}}\left[\frac{1}{Nu_{fs}} + \frac{1}{\beta}\frac{\lambda_f}{\lambda_{solid}}\right]} \qquad \begin{matrix}\beta = 8\\ C = 2.5\end{matrix} \text{ for cylindrical particles}$$

A2.3: Wall heat transfer coefficient

A2.3.1 Dixon (1988)

$$Nu_w = \frac{h_w d_{pv}}{\lambda_f} = \frac{8\beta_s}{d_t/d_{pv}} + Nu_{wf}\left(1 + \beta_s\frac{Pe_{rf}}{\mathrm{Re}_{pv}\mathrm{Pr}}\right) \qquad [70]$$

$\mathrm{Re} > 50$

$$Nu_w = \frac{h_w d_{pv}}{\lambda_f} = \frac{8\beta_s}{d_t/d_{pv}} + 2Bi_s \frac{\lambda_{rs}}{\lambda_f}\frac{d_{pv}}{d_t}\left(1+\frac{\beta_f}{\lambda_{rs}/\lambda_f}\right) \quad \mathrm{Re} < 50$$

The definitions for β_s, β_f, λ_{rs}, Bi_s, Pe_{rf} are given in (Dixon 2 by effective radial conductivity)

A2.3.2 Li & Finlayson (1977)

For cylindrical particles, $20 < \mathrm{Re}_h < 800, 0.03 < d_h/d_t < 0.2$

$$Nu_w = \frac{h_w d_{pv}}{\lambda_f} = 0.18\,\mathrm{Re}_h^{0.93}\,\mathrm{Pr}^{0.33}\frac{d_{pv}}{d_h} \qquad [71]$$

A2.4: Overall heat transfer coefficient

A2.4.1 Dixon (1988)

$$\frac{1}{U_w} = \frac{1}{h_w} + \frac{d_t}{6\lambda_{er}}\frac{Bi+3}{Bi+4} \qquad [72]$$

$$Nu_{fw} = 0.523\left(1-\frac{d_{pv}}{d_t}\right)\mathrm{Pr}^{0.33}\,\mathrm{Re}_{pv}^{0.738}$$

$$Nu_w = \frac{h_w d_{pv}}{\lambda_f} = \frac{8\beta_s}{d_t/d_{pv}} + Nu_{wf}\left(1+\beta_s\frac{Pe_{rf}}{\mathrm{Re}_{pv}\mathrm{Pr}}\right) \quad \mathrm{Re} > 50$$

$$Nu_w = \frac{h_w d_{pv}}{\lambda_f} = \frac{8\beta_s}{d_t/d_{pv}} + 2Bi_s \frac{\lambda_{rs}}{\lambda_f}\frac{d_{pv}}{d_t}\left(1+\frac{\beta_f}{\lambda_{rs}/\lambda_f}\right) \quad \mathrm{Re} < 50$$

$$Bi = \frac{d_t}{2d_{pv}}\frac{Nu_w Pe_{er}}{\mathrm{Re}_{pv}\mathrm{Pr}}$$

The definitions for β_s, β_f, λ_{rs}, Bi_s, Pe_{rf} are given in (Dixon 2 by effective radial conductivity)

A2.4.2 Li & Finlayson (1977)

For cylindrical particles, $20 < \mathrm{Re}_h < 800, 0.03 < d_h/d_t < 0.2$

$$\frac{U_w d_t}{\lambda_f} = 1.40\,\mathrm{Re}_h^{0.95}\,\mathrm{Pr}^{0.33}\exp\left(-\frac{6d_h}{d_t}\right) \quad [73]$$

A2.5 Effective radial diffusivity (D_{er})

A2.5.1 Bauer and Schlünder (1978)

$$D_{er} = \frac{uX_F}{8\left[2-\left(1-2d_{pv}/d_t\right)^2\right]} \quad [74]$$

$$X_F = Fd_{pv}$$

F=1.75 for cylindrical particles

A2.5.2 Rase (1990)

For $d_{pa}/d_t > 0.1$ use $\dfrac{\varepsilon D_{er}}{ud_{pa}} = \dfrac{1}{m} + \dfrac{0.38}{\mathrm{Re}}$ [75]

For $d_{pa}/d_t < 0.1$ divide Der calculated above by $\left[1+19.4\left(\dfrac{d_{pa}}{d_t}\right)^2\right]$

$$m = \begin{cases} 11 & \mathrm{Re} > 400 \\ 57.85 - 35.36\log\mathrm{Re} + 6.68\left(\log\mathrm{Re}\right)2 & 20 < \mathrm{Re} < 400 \end{cases}$$

A2.5.3 Specchia et al. (1980)

$$D_{er} = \frac{ud_{pa}}{8.65\left[1+19.4\left(\dfrac{d_{pd}}{d_t}\right)^2\right]} \quad [76]$$

A2.6 Solid-Fluid heat and mass transfer coefficient

A2.6.1 Gnielinski (1982) & Martin (1978)

$$Nu_{particle} = 2 + F\,\mathrm{Re}_c^{0.5}\,\mathrm{Pr}^{0.33} \quad [77]$$

$$\mathrm{Re}_{pa} = u_f \rho_f d_{pa} \big/ \left(\varepsilon \mu_f\right) \qquad \mathrm{Pr} = \frac{C_p \mu_f}{\lambda_f}$$

$$F = 0.664 \sqrt{\left[1 + \left(\frac{0.0557\,\mathrm{Re}_c^{0.3}\,\mathrm{Pr}^{0.67}}{1 + 2.44\left(\mathrm{Pr}^{0.67} - 1\right)\mathrm{Re}_c^{-0.1}}\right)^2\right]}$$

$$Nu = \left[1 + 1.5\left(1 - \varepsilon\right)\right] Nu_{particle} \frac{d_{pv}}{d_c}$$

$$0.26 < \varepsilon < 0.935 \qquad 0.6 < \mathrm{Pr} < 10000 \qquad \mathrm{Re}_p\,\mathrm{Pr} > 100$$

A2.5.3 Bird et al. (1960)

$$Nu = 2.27\left(1 - \varepsilon\right)^{0.51} \psi^{1.51}\,\mathrm{Re}_h^{0.49}\,\mathrm{Pr}^{0.33} \frac{d_{pv}}{d_h} \quad [78]$$

$$\mathrm{Re}_h \big/ \left(1 - \varepsilon\right) < 300$$

$$Nu = 1.27\left(1 - \varepsilon\right)^{0.41} \psi^{1.41}\,\mathrm{Re}_h^{0.59}\,\mathrm{Pr}^{0.33} \frac{d_{pv}}{d_h} \qquad \mathrm{Re}_h \big/ \left(1 - \varepsilon\right) > 300$$

$\psi = 0.91$ for cylindrical particles

$$\mathrm{Re}_h = \frac{u_f \rho_f d_h}{\mu_f} \qquad \mathrm{Pr} = \frac{C_p \mu_f}{\lambda_f} \qquad Nu = \frac{\alpha_s d_{pv}}{\lambda_f}$$

A2.5.4 Chilton-Colburn analogy (Westerterp, 1984)

$$Nu = Sh\left(\frac{\mathrm{Pr}}{Sc}\right)^{\frac{1}{3}} \quad [79]$$

Wilke & Hougen (Berty, 1999)

$$j_h = 1.95\,\mathrm{Re}_p^{-0.51}$$

$$j_d = 1.82\,\mathrm{Re}_p^{-0.51}$$

Where:

$$\mathrm{Re}_p = Gd_p/\mu \quad \text{for } \mathrm{Re}_p < 350$$

With:

$$j_h \equiv St\,\mathrm{Pr}^{0.66}$$

$$j_d \equiv St'Sc^{0.66}$$

A2.5.5 Heat Peclet number

To describe the dimensionless effective radial thermal conductivity to following can be applied (Koning, 2002):

$$\frac{\lambda_{e,r}}{\lambda_f} = \frac{\lambda_r^0}{\lambda_f} + \frac{Pe_h^0}{Pe_{h,r}^{\infty}} \qquad [80]$$

Where:

- Molecular Peclet number: $Pe_h^0 = \dfrac{u_0 \rho_f C_{p,f} d_p^v}{\lambda_f}$
- Peclet number dependant on the aspect ratio: $Pe_{h,r}^{\infty} = 8\left[2 - \left(1 - \dfrac{2}{N}\right)^2\right]$
- Aspect ratio: $N = \dfrac{D_t}{d_p^v}$

A2.5.6 Mass Peclet number (Fahien, 1955)

Radial mass transfer for packings of different shapes.

$$Pe_{m,r}^{\infty} = C\left[1+\frac{19.4}{N^2}\right] \quad [81]$$

Where:

- $C = 8.65\frac{d_p^v}{d_p^a}$
- Aspect ratio: $N = \frac{D_t}{d_p^a}$
- Volume equivalent diameter of sphere with same diameter as surface area of particles in the packing $d_p^a = d\sqrt{\frac{1}{2}+\frac{h}{d}}$

A2.7 Axial dispersion of heat and mass

A2.7.1 Edwards & Richardson (1968)

Mass dispersion

$$\frac{1}{Pe_{mz}} = \frac{0.73\varepsilon}{\mathrm{Re}\,Sc} + \frac{0.5}{\left(1+\frac{9.7\varepsilon}{\mathrm{Re}\,Sc}\right)} \quad [82]$$

$0.008 < \mathrm{Re} < 50, 0.0377 < d_p < 0.6cm$

A2.7.2 Wen & Fan (1975)

$$\frac{1}{Pe_{mz}} = \frac{0.3}{\mathrm{Re}\,Sc} + \frac{0.5}{\left(1+\frac{3.8}{\mathrm{Re}\,Sc}\right)} \quad [83]$$

$0.008 < \mathrm{Re} < 400, 0.28 < Sc < 2.2$

A2.7.3 Bischoff & Levenspiel (1962)

$$\frac{1}{Pe_{mz}} = \frac{\varepsilon}{\tau \operatorname{Re} Sc} + \frac{0.45}{\left(1 + \frac{7.3}{\operatorname{Re} Sc}\right)} \quad [84]$$

A3: Thermal Properties

A3.1 Thermal conductivity

The thermal conductivity of species present in the system has to be evaluated to be used in the modelling of the system. A relatively large part of the reactor consists of open space and thus heat transfer due to forced convection will have a big influence on the effective overall heat transfer of the system. The following temperature dependant equation was used to evaluate the individual thermal conductivity:

$$k_{g,i} = A + B.T + C.T^2 \quad [85]$$

The following table supplies coefficients A, B and C for the various gas species (Yaws, 1999).

Table A-1: Thermal conductivity coefficients

	A	B	C
SO_3	-0.00354	5.02×10^{-5}	-5.55×10^{-9}
SO_2	-0.00394	4.48×10^{-5}	2.11×10^{-9}
O_2	-0.00121	8.62×10^{-5}	-1.33×10^{-8}
H_2O	0.00053	4.71×10^{-5}	4.96×10^{-8}
N_2	0.008	6.00×10^{-5}	-5×10^{-9}

The combined thermal conductivity of the various gases was evaluated by using the following equation:

$$\lambda_{m,f} = \sum \frac{y_i \lambda_i}{\sum y_i A_{ij}} \quad [86]$$

Where:

$$A_{ij} = \frac{1}{4}\left\{1+\sqrt{\frac{\mu_i}{\mu_j}\left(\frac{M_j}{M_i}\right)^{\frac{3}{4}}\left(\frac{T+S_i}{T+S_j}\right)}\right\}^2 \left(\frac{T+S_{ij}}{T+S_i}\right) \quad [87]$$

$$S_i = 1.5 * T_{bi} \quad [88]$$

$$S_{ij} = S_{ji} = C\left(S_i S_j\right)^{0.5} \quad [89]$$

A3.2 Dynamic Viscosity

The dynamic viscosity in the packed bed needs to be evaluated in order to account for the resistance caused by friction due to flow. The dynamic viscosity was needed to evaluate the reactor models. The following equation was used to determine the individual dynamic viscosities:

$$\mu_{g,i} = A + B.T + C.T^2 \quad [90]$$

The following table supplies the coefficients for all the species to be used in equation (Yaws, 1999).

Table A-2: Dynamic viscosity coefficients

	A	B	C
SO_3	-12.039	$5.43x10^{-1}$	$-1.60x10^{-4}$
SO_2	-11.103	$5.02x10^{-1}$	$-1.08x10^{-4}$
O_2	44.224	$5.62x10^{-1}$	$-1.13x10^{-4}$
H_2O	-36.826	$4.29x10^{-1}$	$-1.62x10^{-4}$
N_2	$9x10^{-6}$	$4x10^{-8}$	$-4x10^{-12}$

The combined heat dynamic viscosity from all species was calculated by the following:

$$\mu_{m,f} = \sum \frac{y_i \mu_i}{\sum y_i \phi_{ij}} \quad [91]$$

Where:

$$\phi_{ij} = \frac{\left[1+\left(\mu_i/\mu_j\right)^{0.5}\left(M_j/M_i\right)^{0.25}\right]^2}{\left[8\left(1+M_i/M_j\right)\right]^{0.5}} \quad [92]$$

$$\phi_{ji} = \left(\mu_j/\mu_i\right)\left(M_i/M_j\right)\phi_{ij} \quad [93]$$

A3.3 Heat Capacity

The amount of energy required to change the temperature of any substance by a desired amount i.e. heat capacity was evaluated to account for the change in temperature due to heat flux from the wall, as well as dissipation of heat due to reaction. The following equation was used to evaluate the heat capacity:

$$C_p = A + B.T + C.T^2 + D.T^3 + \frac{E}{T^2} \quad [94]$$

The following table supplies coefficients for all gas species to be used in equation 94 above.

Table A-3: Heat capacity coefficients

	A	B	C	D	E
SO_3	24.025	119.461	-94.387	26.962	-0.116
SO_2	21.430	74.351	-57.752	16.355	0.087
O_2	29.659	6.137	-1.187	0.096	-0.220
H_2O	30.092	6.833	6.793	-2.534	0.082

N_2	19.5	19.88	-8.598	1.369	0.5276

The combined heat capacity was the sum of the each species multiplied by the molar fraction:

$$c_{p,m} = \sum y_i c_{p,i} \quad [95]$$

A3.4 Density

The density of the various species was calculated using the ideal gas law. The following equation was used to account for each of the individual gas species:

$$\rho_i = \frac{P.M_{w,i}}{R.T} \quad [96]$$

A3.5 Titanium Dioxide

The TiO_2 used in this study contains 75% anatase and 25% rutile phase as already mentioned. The solid density was taken as the combined fraction of each phase multiplied by that specific density. A density of 2 406 kg/m^3 was obtained for a void fraction of 0.39 evaluated from BET analysis. Incropera & De Witt (2002) supplies thermal conductivity and heat capacity values at different temperatures. These values were used by fitting a second order polynomial through the data. The following two equations were used to represent the heat capacity and thermal conductivity of TiO_2:

$$k_s = 8e^{-6}T^2 - 0.0166T + 12.37 \quad [97]$$

$$c_{p,s} = 4e^{-7}T^3 - 0.0012T^2 + 1.2798T + 464 \quad [98]$$

A3.6 Heat of Reaction

The heat of reaction is the energy required to thermodynamically split a molecule of SO_3 into SO_2 and 0.5 O_2. The heat of reaction given at reference temperature is 98.92 kJ/mol (T_R = 298 K). To account for the operating temperature the change in heat capacity will account for the change in heat absorbed to

decompose SO_3. The following equation can be utilized to describe the heat of reaction at changing operating temperature conditions (Smith, 2001):

$$\Delta H_{Rx}(T) = \Delta H^{0}_{Rx}(T_R) + \int_{T_R}^{T} \Delta c_p dT \qquad [99]$$

A4: GC calibration Standard Gases

The standard GC calibration gases were obtained from AFROX and Table A-4 includes volume/molar percentage of the gas sample content.

Table A-4: GC calibration standard gases

Gas	SO_2	O_2	N_2
1	1	0.5	98.5
2	10	5	85
3	50	25	25

B. Appendix B: Micro Pellet Reactor Model

B1: Physical Properties

The physical values for all parameters used in the CFD model can be found in Table B-1:

Table B-1: Catalyst pellet CFD model parameter values

	Fluid					Solid			
Parameter	**923**	**973**	**1023**	**1 073**	**Parameter**	**923**	**973**	**1 023**	**1 073**
Concentration									
ρ_b	100	100	100	100	ε_p	0.16	0.16	0.16	0.16
D_{eff}	4.65e-5	5.19e-5	5.6e-5	6.1e-5	ρ_b	2520	2520	2520	2520
C_{a0}	0.98	0.93	0.89	0.85	D_{efs}	4.72e-5	5.19e-5	5.2e-5	4.85e-5
C_{b0}	0	0	0	0	C_{as0}	0	0	0	0
C_{c0}	0	0	0	0	C_{bs0}	0	0	0	0
C_{i0}	0.74	0.72	0.69	0.65	C_{cs0}	0	0	0	0
C_{n0}	10.06	9.5	9.04	8.62	C_{is0}	0	0	0	0
					C_{ns0}	0	0	0	0
					D_k	4.95e-6	5.07e-6	5.2e-6	5.32e-6
					$D_{eff,m}$	4.3e-7	4.5e-7	4.64e-7	4.7e-7
					τ	1.43	1.43	1.43	1.43
Thermal									

λ_f	0.06	0.062	0.065	0.069	λ_s	3.5	3.5	3.5	3.5
λ_{gw}	0.1	0.1	0.1	0.1	$c_{p,s}$	900	905	910	915
$\bar{M}_w$	0.019	0.019	0.019	0.019	$T_{s,0}$	923	973	1023	1073
$c_{p,f}$	34.59	34.12	34.48	35.77	ρ_s	2520	2520	2520	2520
T_0	923	973	1023	1073					
P_0	87.3	87.3	87.3	87.3					
ρ_f	0.34	0.316	0.30	0.293					
μ_f	4e-5	4.2e-5	4.38e-5	4.53e-5					

B2: Particle Sizes

Table represents the physical sizes of the particles used in the experiments and model together with some experimental values.

Table B-2: Catalyst pellet sizes used in experiments and model

	1	**2**	**3**	**4**	**5**	**T (^oC)**	**U (m/s)**	**Ra ($mol/m^3.s$)**	**WHSV (h^{-1})**
hp	4.7	5.1	4.48	4.12	4.1	750	0.95	144.85	60
dp	1.6	1.68	1.56	1.6	1.82				
2									
hp	4.12	4.1	4.56	5.02	3.9	750	0.95	299.7	178

dp	1.68	1.66	1.6	1.6	1.52				
3									
hp	3.94	4.14	3.94	3.96	5.17	750	0.95	336	320
dp	1.6	1.68	1.68	1.64	1.56				
4									
hp	4.28	4.74	4.86	4.96	4.78	750	0.95	322	343
dp	1.64	1.62	1.56	1.66	1.6				
5									
hp	4.14	4.74	4.96	5.16	4.36	800	1	159	56
dp	1.52	1.63	1.64	1.6	1.6				
6									
hp	4.2	5.22	5.12	4.96	5.1	800	1	468	268
dp	1.61	1.64	1.62	1.55	1.54				
7									
hp	4	4.52	3.88	5	4.5		1	560	391
dp	1.52	1.56	1.6	1.6	1.72	800			
8									
hp	5.1	3.8	4.21	4.96	3.34	800	1	336	182
dp	1.64	1.66	1.64	1.54	1.66				
9									
hp	3.6	4.7	4.12	5.6	3.98	700	0.91	111	66

dp	1.58	1.58	1.42	1.58	1.6				
10									
hp	5.3	4.56	5	5.02	3.9	700	0.91	163	171
dp	1.6	1.58	1.64	1.58	1.68				
11									
hp	4.33	5.42	5.2	4.1	5.1	700	0.91	176	272
dp	1.66	1.64	1.66	1.66	1.7				
12									
hp	4.54	5	5.6	5.08	4.59	700	0.91	171	326
dp	1.4	1.88	1.66	1.64	1.58				
13									
hp	4.66	4.54	4.38	4.68	5.2	650	0.86	50	57
dp	1.64	1.72	1.58	1.56	1.62				
14									
hp	5.14	5.1	4.48	4.35	4.54	650	0.86	94	170
dp	1.6	1.62	1.66	1.63	1.65				
15									
hp	4.22	4.42	5	4.74	4.98	650	0.86	91	294
dp	1.6	1.58	1.68	1.58	1.6				
16									
hp	4.84	4.14	5.34	5.6	4.12	650	0.86	67	327

dp	1.6	1.58	1.68	1.72	1.58				

B3: Supplementary CFD Results

Additional results generated in the catalyst pellet model using COMSOL Multi-Physics® 4.3b include velocity distribution and concentration distribution. Velocity distribution can be seen in Figure B-1.

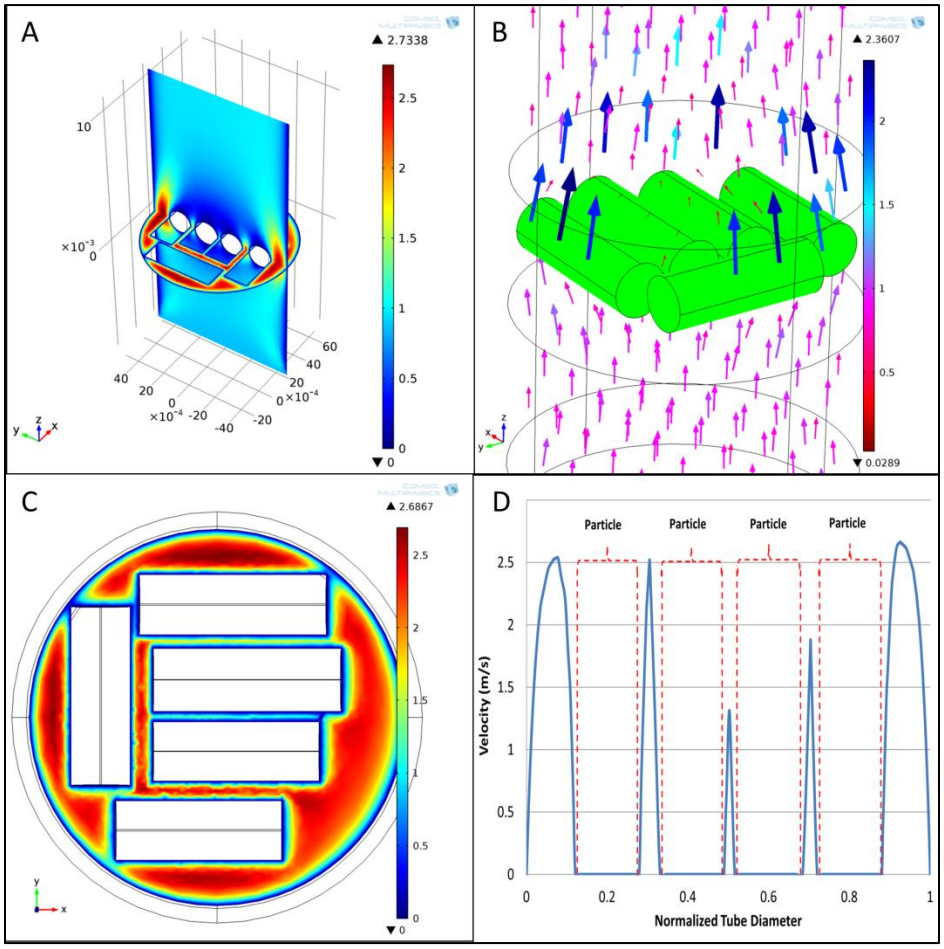

Figure B-1: Model Results; A: Cross sectional (axial & radial) velocity distribution (m/s); B: Streamline velocity distribution through the porous media (m/s); C: Cross sectional (radial) velocity distribution (m/s); D: Centreline velocity profile (m/s)

Concentration distribution of sulphur trioxide (A), sulphur dioxide (B) and oxygen (C) can be seen in Figure B-2.

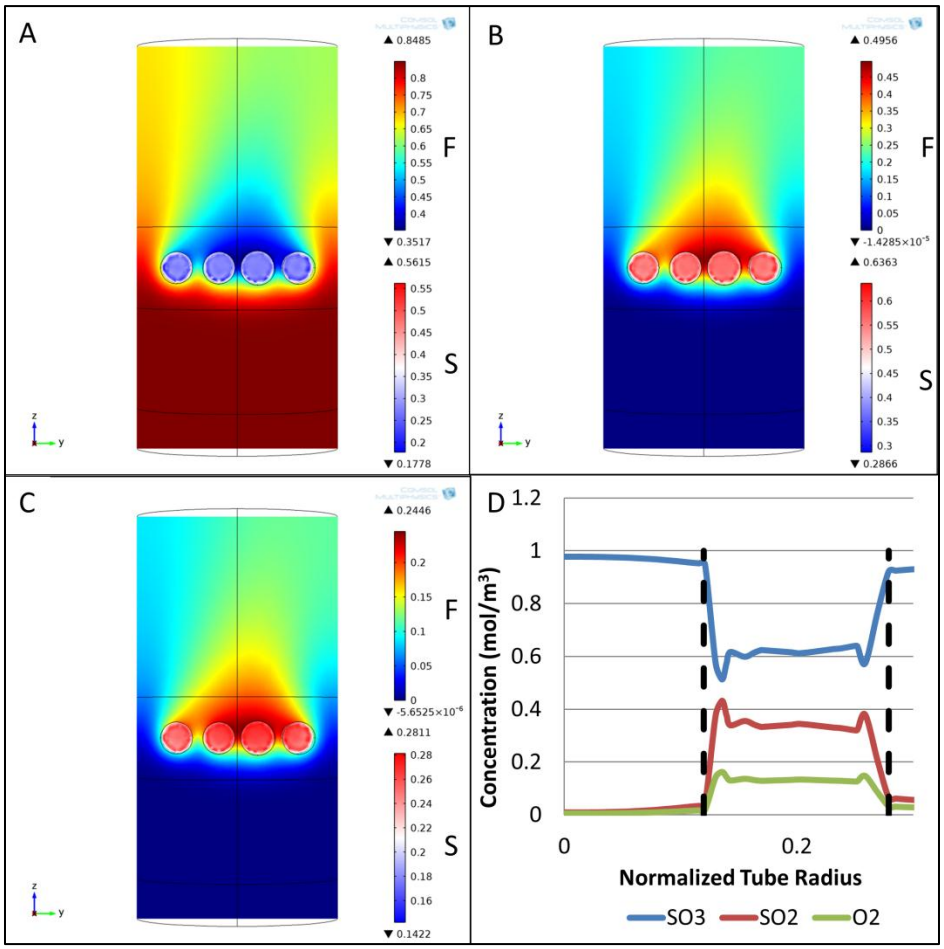

Figure B-2: 2D Cross sectional results for concentration 1 at temperature 1 073 K inlet; A: Concentration distribution of SO_3 (mol/m^3); B: Concentration distribution of SO_2 (mol/m^3); C: Concentration distribution of O_2 (mol/m^3); D: Centreline concentration profile through fluid and one particle (F indicates fluid phase and S solid phase)

Concentration distribution on the surface of the catalyst particles for sulphur trioxide (A), sulphur dioxide (B) and oxygen (C) can be seen in Figure B-3.

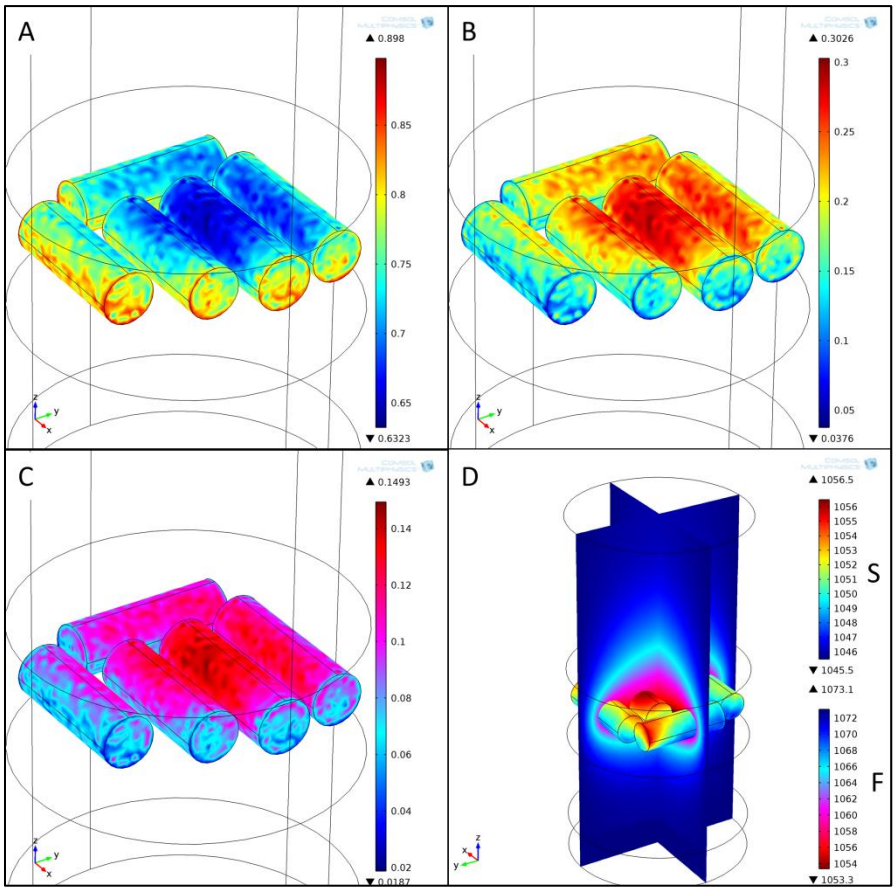

Figure B-3: Distribution on surface of particles; A: Concentration of SO_3 (mol/m^3); B: Concentration of SO_2 (mol/m^3); C: Concentration of O_2 (mol/m^3); D: Temperature distribution on surface of particles as well as fluid (K) (F indicates fluid phase and S solid phase)

C. Appendix C: Porosity and Void Fraction Calculations

The definition of porosity is said to be the volume of open pores per total volume of solid (Gregg, 1982). The porosity of a porous catalyst particle can be evaluated by N_2 or CO_2 physi-sorption by BET analysis. In order to determine this porosity the incremental volume change absorbed per pore width range has to be integrated over the entire pore range. This can be accomplished by using the following equation:

$$\varepsilon_0 = \rho_b \int \left(\frac{dV}{dD_{pore}} \right) dD_{pore} \qquad [100]$$

The BET analysis was completed by UCT. The bulk density was evaluated by inserting an amount of catalyst in a 50 mL measuring flask with the same inner diameter as the reactor. The flask was filled with catalyst up to the 50 mL mark. The amount of catalyst was weighed without moving the flask as to ensure the same random packing. This was done for six times to get an average weight per volume flask. This resulted in a bulk density of 995 kg/m^3 and a particle density (Taking TiO_2 density of 4000 kg/m^3) of 2 443 kg/m^3. Dividing the bulk density by the particle density, the void fraction for the reactor was found to be 0.4074. This value was compared to a theoretical equation used to evaluate the void fraction for cylindrical particles. The following equation was used (Adams, 2009):

$$\varepsilon_b = 0.38 + 0.073 \left[1 - \frac{\left(d_t/d_p - 2 \right)^2}{\left(d_t/d_p \right)^2} \right] \qquad [101]$$

The equation gave a void fraction of 0.4012. This equation gives an accurate representation of the void fraction in the bed with an error of 1.67% for the values of the fresh catalyst. The results obtained for void fractions of particle and bed can be seen in Table C-1.

Table C-1: Void fraction and particle density

	Fresh	Spent
ρ_B (kg/m^3)	995	1177
ρ_p (kg/m^3)	2443	3325

ε_b	0.4074	0.35
ε_0	0.3892	0.2012

D. Appendix D: Heat and Mass Transfer Criteria

The fluid flow around the particle with the interaction of heat and mass between the fluid phase and the solid phase can simplify or complicate reactor modelling and kinetic evaluation of a catalyst. As mentioned in Chapter 2 certain criteria can be used to eliminate certain effects on the catalyst an in turn simplify the numerical mathematical model to be solved. During this study different forms of the catalyst was utilized, including:

- Single solid catalyst particles
- A packed bed of particles

The criteria of Mears as mentioned in Chapter 2 will be discussed with relation to the experimental conditions for the three different scenarios mentioned above.

D1: Overall Particle Model

The 5 catalyst pellets were used to evaluate the kinetics for the reaction and the influence of heat and mass transfer were evaluated. The conditions and values for concentration 1 are given in the following tables. Due to the amount of data and similarities other experimental runs criteria will not be given.

Table: D-1: Interfacial gradients for particles (Concentration 1)

	Temperatures				**Unit**
	923	**973**	**1023**	**1073**	**K**
r_{eff}	91	176	336	468	mol/m^3.s
C_{A0}	0.99	0.94	0.89	0.85	mol/m^3
k_s	0.95	0.96	0.94	0.96	m/s
n	1	1	1	1	-
h_s	75	64	67	65	W/m^2.s
Ar	25.54	24.23	23.04	21.97	

Heat Criteria	2.6	5.2	9.2	11.6	
Mass Criteria	0.08	0.15	0.28	0.45	

The criteria for concentration and heat gradients between the fluid and solid are given as:

$$\left|\frac{r_{eff} d_p}{2C_{A0} k_s}\right| < \frac{0.15}{n} \quad [102]$$

$$\left|\frac{-\Delta H_{Rx} r_{eff} d_p}{2T_0 h_s}\right| Ar < 0.15 \quad [103]$$

Intra-particle gradients

Table D-2: Intra-particle gradients for particles (Concentration 1)

	Temperatures				**Unit**
	923	**973**	**1023**	**1073**	**K**
D_{eff}	6.5x10-7	1.66x10-6	4.5x10-7	1.49x10-7	m^2/s
C_s	0.99	0.94	0.89	0.85	mol/m^3
λ_c	3.5	3.5	3.5	3.5	W/m.K
T_s	923	973	1023	1073	K
T_c	922.98	972.9	1022.9	1073	K
Criteria	91	67	571	2374	

The intra-particle mas and heat transfer gradients can be neglected if the following is true:

$$Da_{II} \left| n - Ar.P_t \right| < 1 \quad [104]$$

Where the Damkohler group 2 which gives the ratio between chemical rate and molecular diffusion and Prater number (maximum intra-particle temperature rise):

$$Da_{II} = \frac{r_{eff} d_p^2}{4 D_{eff} C_s} \quad [105]$$

$$P_t = \frac{-\Delta H_{Rx} D_{eff} C_s}{\lambda_e T_s} \quad [106]$$

From the criteria used to describe concentration 1 (Chapter 4) it can be seen (Table: D-1 & Table D-2) that the criteria are satisfied for an inlet temperature 923K. Al the other criteria are not satisfied which means inter and intra-particle heat and mass transfer effects are prominent.

D1.2 Effect of Pore Diffusion

To determine if the diffusion inside of the catalyst particles are limiting the Wagner-Weisz-Wheeler modulus can be used with measured quantities to indicate whether this effect is severe (Levenspiel, 1999):

$$M_w = L^2 \frac{\left(-r_A''' / C_A\right)_{obs}}{D_e} \quad [107]$$

When $M_w < 0.15$ the particles are in diffusion-free regime while if $M_w > 4$ the particles are in a strong pore diffusion regime.

Table D-3: W-W-W criteria for pore diffusion

	Temperature		**Units**
	923	**1073**	**K**
Criteria	22.9	593	

The WWW modulus was evaluated for the highest and lowest temperature of concentration 1 and it was found that there were strong resistance to pore diffusion. The results for concentration 2 are not shown since similar results were obtained.

D2: Packed Bed Model

The packed bed consisted of a bed of particles where the aspect ratio was approximately 13. The criteria for interfacial gradients, as well as intra-particle gradients were evaluated in the same manner as for the particle model described above. Two additional gradient evaluations have to be conducted for the large fixed bed which includes axial and radial dispersion of heat and mass. Axial dispersion in a packing may be as a result of the packing structure that the mixing of the fluid becomes severe. To evaluate this effect the Mears criterion was used to evaluate whether axial dispersion should be accounted for. The following criteria can be used to determine if this effect is negligible:

$$\left| \frac{n.Da_I}{Pe_{a,m}} - \frac{Ar.Da_{III}}{Pe_{a,h}} \right| < 0.05 \qquad [108]$$

Where:

- $Da_I = \frac{r_{eff} d_p}{u_s C_{a0}}$; Damkohler group 1
- $Da_{III} = \frac{-\Delta H_{Rx} r_{eff} d_p}{\rho_f u_s T_w c_p}$; Damkohler group 3
- $Pe_{a,m} = \frac{u_s d_p}{D_a}$; Peclet number for mass
- $Pe_{a,h} = \frac{\rho_f u_s d_p c_p}{\lambda_a}$; Peclet number for heat

If the condition is satisfied axial dispersion may be neglected from the model. The next criterion are that for radial dispersion of heat and mass. The effects of radial dispersion are quite an important one as it has the possibility to reduce a model with a dimension; from 2D to 1D. The criterion are as follows:

$$\left| \frac{-\Delta H_{Rx} r^*_{eff} d_t^2}{\lambda_r T_w} \right| .Ar < \frac{1.6}{1 + \frac{8}{Bi_w}} \qquad [109]$$

Where:

- $Bi_w = \frac{\alpha_w d_t}{\lambda_{eff,r}}$

The mass and heat dispersion coefficients in the axial direction were calculated by the correlations provided by Wen & Fan (1975) and Dixon and Cresswell (1979) respectively. Effective radial thermal conductivity was equated by Bauer and Schlünder (1978) and radial diffusivity was also equated by Bauer and Schlünder (1978).

Interfacial gradients:

Table D-4: Interfacial gradients for packed bed

	Temperatures		**Unit**
	903	**1053**	**K**
r_{eff}	4.83	8.05	mol/m^3.s
C_{A0}	3.19	1.81	mol/m^3
k_s	0.205	0.237	m/s
n	1	1	-
h_s	280	287	W/m^2.s
Ar	26.11	22.39	
Heat Criteria	0.03	0.07	
Mass Criteria	0.0093	0.0237	

Intra-particle gradients:

Table D-5: Intra-particle gradients for packed bed

	Temperatures		**Unit**
	903	**1053**	**K**

D_{eff}	$1.43x10^{-7}$	$1.6x10^{-7}$	m^2/s
C_s	3.19	1.81	mol/m^3
λ_c	3.5	3.5	W/m.K
T_s	903	1053	K
T_c	902.9	1052.9	K
Criteria	16.74	43.85	

Axial Dispersion:

Table D-6: Axial dispersion criteria for packed bed

	Temperatures		**Units**
Parameter	**903**	**1053**	**K**
Da_I	$1.71x10^{-3}$	$2.26x10^{-3}$	-
Da_{III}	0.0017	0.0022	-
Pe_{am}	0.18	0.18	-
Pe_{ah}	1.75	1.72	-
u_s	1	1.32	m/s
ρ_g	0.58	0.50	kg/m^3
C_p	1843	1905	J/kg.K
T_w	903	1053	K

D_a	0.0149	0.0188	m^2/s
λ_a	1.12	1.23	W/m.K
Criteria	0.004	0.005	

Radial Dispersion:

Table D-7: Radial dispersion criteria for packed bed

	Temperatures		**K**
	903	**1053**	**Units**
r^*_{eff}	5.8	9.6	$mol/m^3.s$
λ_r	59.1	65.9	W/m.K
Bi_w	0.27	0.27	-
α_w	766	854	$W/m^2.K$
$\lambda_{eff,r}$	60.19	66.9	W/m.K
Pe_r	11.39	11.39	-
d_t	0.0209	0.0209	m
N	8.31	8.31	-
Criteria	0.12	0.14	

E. Appendix E: Thermodynamic Equilibrium Conversion

E1: Kinetic Setup Equilibrium Conversion

The sulphur trioxide decomposition reaction is a reversible reaction and thus at specific reaction conditions the forward and backward rate of the reaction will be the same. The sulphur trioxide equilibrium conversion without any inert species and with nitrogen as inert carrier was calculated thermodynamically to evaluate whether the system is close to equilibrium conditions.

***Pure SO_3 equilibrium conversion**:*

The method in Smith and Van Ness (Smith, 2001) was used to do evaluate the equilibrium conversion curves at different pressure as a function of temperature. The equation given for equilibrium constant includes Gibbs energy, Heat of reaction and Heat capacity as follows:

$$\ln K = -\frac{\Delta G^o}{RT} \qquad [110]$$

Where:

$$\frac{\Delta G^o}{RT} = \frac{\Delta G_0^o - \Delta H_0^o}{RT_0} + \frac{\Delta H_0^o}{RT} + \frac{1}{T}\int_{T_0}^{T} \frac{\Delta C_p^0}{R} dT - \int_{T_0}^{T} \frac{\Delta C_p^0}{R} \frac{dT}{T} \qquad [111]$$

The equilibrium expression displaying the pressure and composition is given as:

$$\prod \left(y_i \hat{\phi}_i \right)^{v_i} = \left(\frac{P}{P_0} \right)^{-v} K$$

[112]

In Equation 112 above the pressure divided by the standard pressure of 1 bar to the power of the total molar fraction of system. This is equal to the sum of the molar fraction of species multiplied by the fugacity for that specie. The fugacity of species was calculated by the following equation:

$$\phi = \exp\left(\frac{P_r}{T_r} \left(B^0 + \omega B^1 \right) \right) \qquad [113]$$

With:

$$B^0 = 0.083 - \frac{0.422}{T_r^{1.6}} \quad [114]$$

$$B^1 = 0.139 - \frac{0.172}{T_r^{4.2}} \quad [115]$$

All the values needed for pure species is obtained in tables from Smith and Van Ness. The following figure was generated using the equations given above to determine the equilibrium conversion as a function of temperature at different pressures:

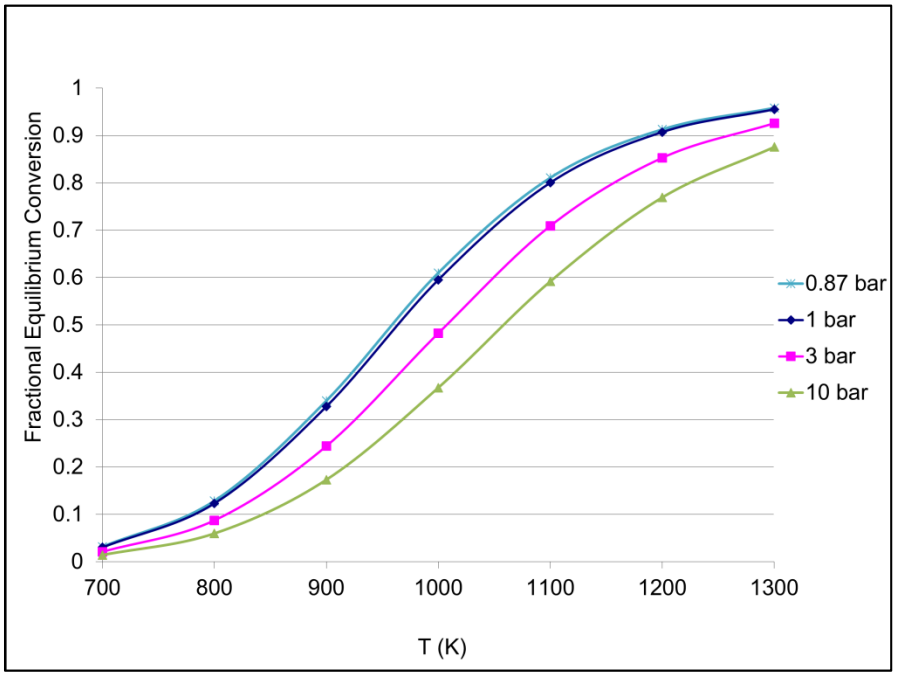

Figure E-1: Equilibrium conversion for pure SO_3 at different pressure as a function of temperature

H_2SO_4 equilibrium conversion with inert Nitrogen:

The total decomposition of H_2SO_4 is a very difficult objective to quantify experimentally as the acid in decomposed form, SO_3 and H_2O, has the tendency in the absence of heat to combine and form acid again. In the work of Kondamudi & Upadhyayula (2010) they did some simulations on Aspen HYSYS V7.1 using a Gibbs type reactor with the Peng-Robinson-Stryjek-Vera and modified Peng-Robinson equation of state so that ideal gas approximation need not be used. The same approach was followed during this study to determine the equilibrium conversion and the shift in equilibrium conversion due to the

presence of inert nitrogen in the feed stream. The SRK equation of state and NRTL was used to evaluate the equilibrium conversion. The first simulation entailed the equilibrium conversion of pure sulphuric acid at different temperatures. The following figure depicts conversion of pure sulphuric acid as a function of temperature at different pressures.

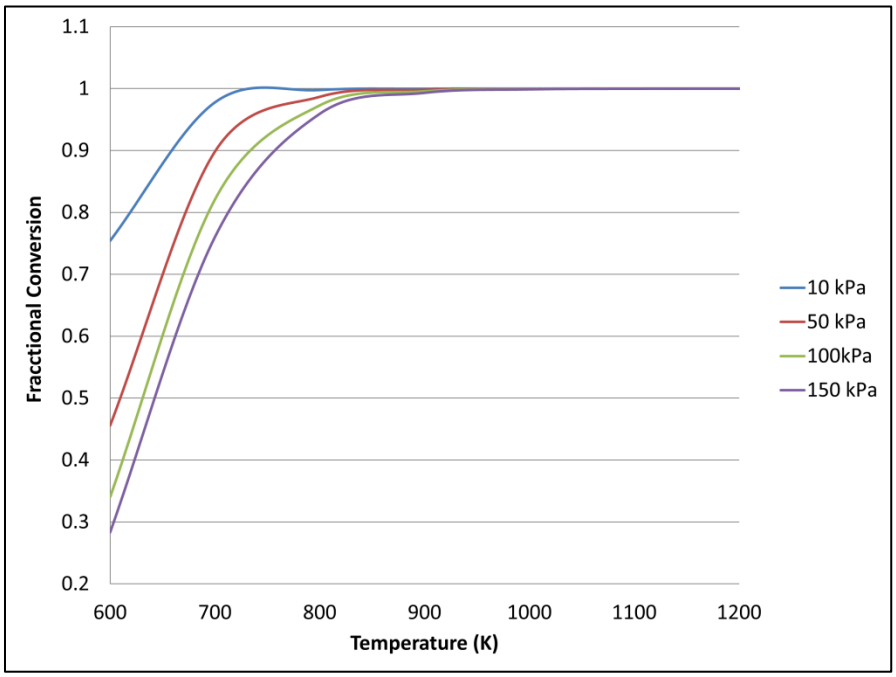

Figure E-2: Equilibrium conversion for pure H_2SO_4 at different pressure as a function of temperature

The experimental setup, however, does not only contain pure H_2SO_4 but also inert nitrogen to increase flow rate to ensure enough flow goes through to the gas analyser, to dilute the gas stream due to the limitations of percentage gas analysed in the gas analyser and to ensure WHSV can be increased without increasing acid flow and possibly cause overflow in traps. The same approach was followed and the following graph represents the decomposition of H_2SO_4 and nitrogen in the molar ratio as in the catalyst experiments.

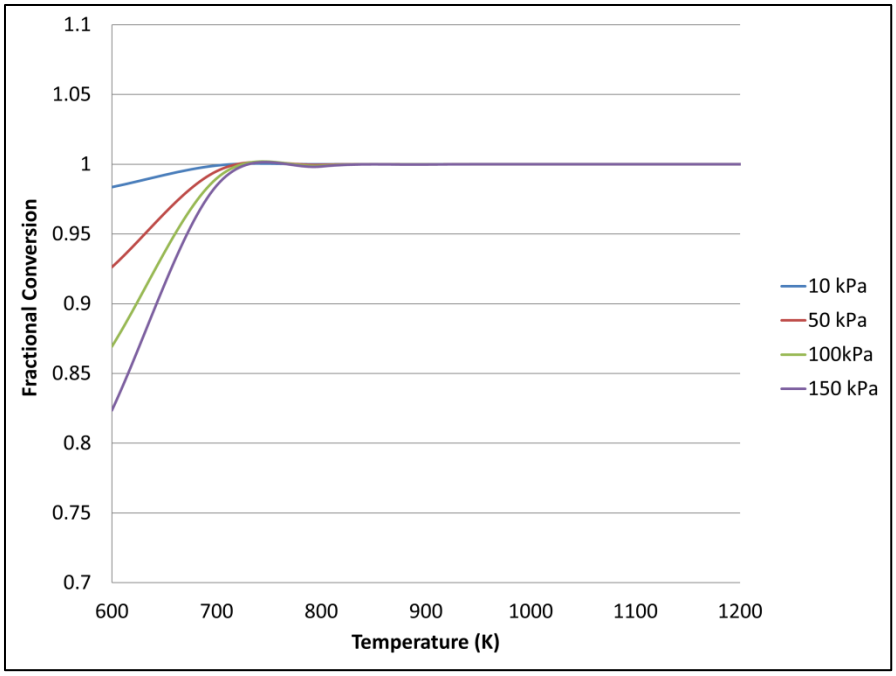

Figure E-3: Equilibrium conversion of H_2SO_4 with inert nitrogen

For the sulphuric acid decomposition reaction the NRTL equation of state was used. From Figure E-3 and Figure E-2 it can be seen that the inert nitrogen shifts the equilibrium conversion and enhances the decomposition reaction due to the principle of Le Chatelier. Thus with the flow conditions of the kinetic setup the assumption can be valid that all sulphuric acid is decomposed at start of catalyst bed and only SO_3 and H_2O present.

SO_3 with inert nitrogen for powder kinetics:

The influence of nitrogen on the equilibrium conversion was calculated thermodynamically. Various equations of state were used in simulations but did not differ to a great extent. For the specific molar feed ratio of SO_3, H_2O and N_2 the equilibrium conversion for different pressures as a function of temperature can be seen in Figure E-4.

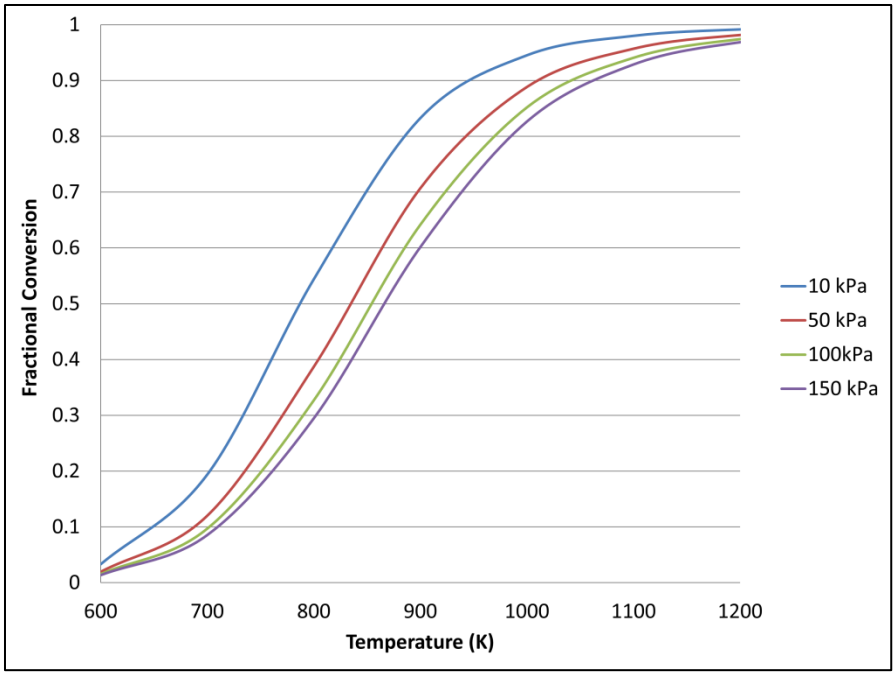

Figure E-4: Equilibrium conversion of feed composition to differential bed at different pressure as a function of temperature

The reason for only evaluating equilibrium conversion at low pressure is that for the kinetic setup the process conditions were chosen to be atmospheric and the setup used could not work under pressure due to the quartz couplings not being able to withstand high pressure. From Figure E-3 and Figure E-4 it can be seen that inert nitrogen increases the equilibrium conversion by a significant margin. The results obtained from Aspen HYSYS simulations compared very well with the work from *Kondamudi & Upadhyayula (2010).*

SO_3 with inert nitrogen for particle kinetics:

The equilibrium conversion was equated as described above for the particle kinetics process conditions. The variable was the inlet concentration and the temperature. Thus the pressure was taken to be constant as 83.7 kPa throughout. The results obtained can be seen in Figure E-5 for the equilibrium conversion as a function of temperature for the 4 different inlet conditions.

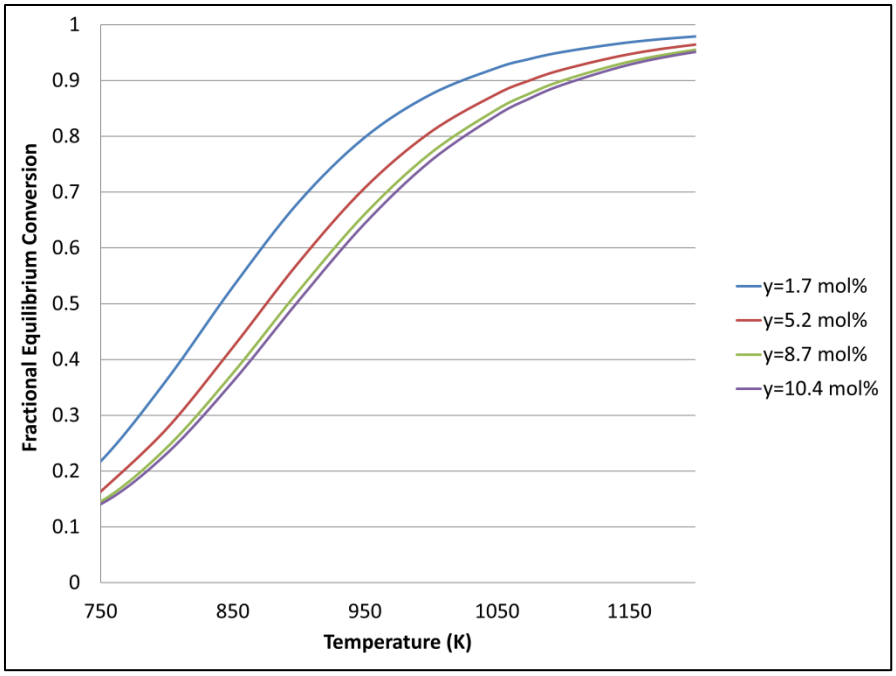

Figure E-5: Equilibrium conversion of particle kinetics for different inlet concentrations as a function of temperature and constant inlet pressure

E2: Packed Bed Setup Equilibrium Conversion

Variable WHSV:

The equilibrium conversion was equated in the same manner as described in Section E.1 above in an Aspen Model. In this section some equilibrium graphs were generated for the variation in WHSV, specifically the 3 and 4 ml/min acid flow rates. These graphs can be seen in Figure E-6 and Figure E-7 where the equilibrium conversion is given as a function of temperature for different operating pressure. Since the process conditions of the fixed bed system varied much and specifically the amount of pre-conversion achieved, as well as the operating temperature, the equilibrium conversion was equated for all individual experimental results. All the data will not be given here but the specific values are given in the applicable graphs in Chapter 6.

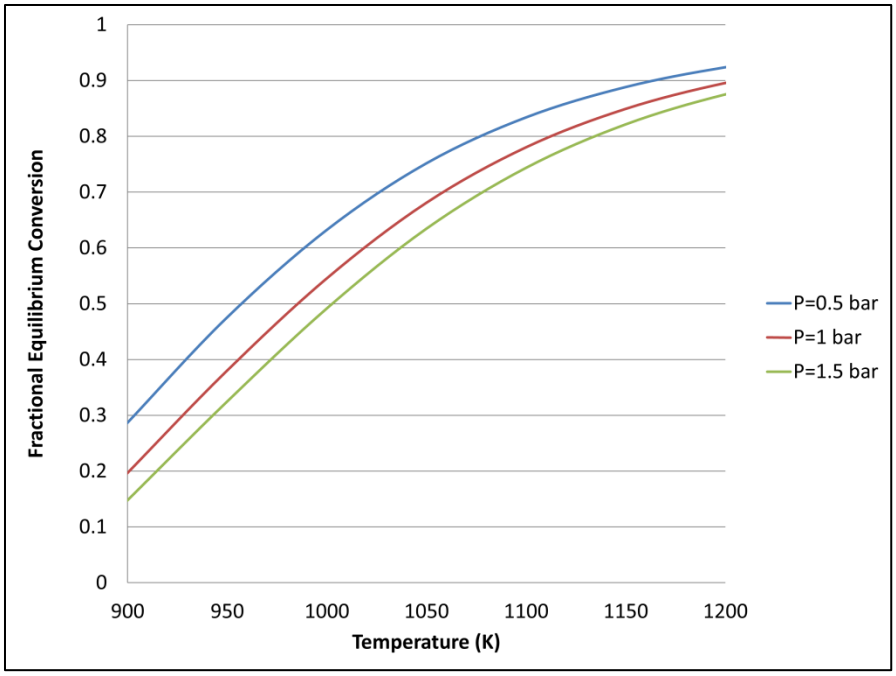

Figure E-6: Equilibrium conversion for variable WHSV process conditions as a function of pressure (Acid=3 ml/min)

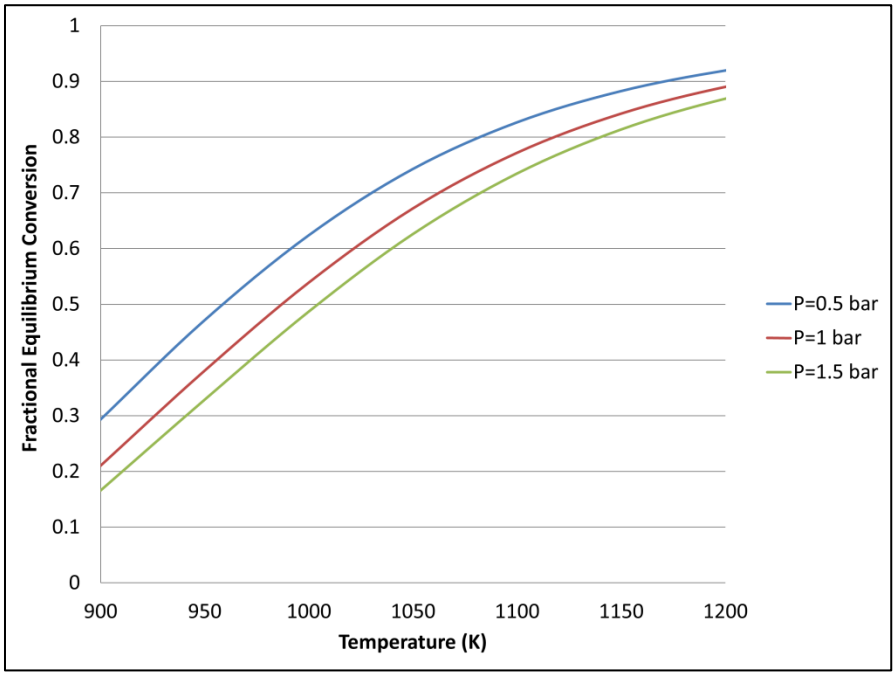

Figure E-7: Equilibrium conversion for variable WHSV process conditions as a function of pressure (Acid=4 ml/min)

F. Appendix F: Reactor Equations

The equations used in the CFD models for the systems are given below in cylindrical coordinates, represented by the Nabla operator in the Chapters.

F1: 3D Particle Model

Solid Phase:

$$D_{efm,r}\left(\frac{\partial^2 C_{s,r}}{\partial r^2}+\frac{1}{r}\frac{\partial C_{s,r}}{\partial r}\right)+D_{efm,\phi}\frac{1}{r^2}\frac{\partial^2 C_{s,\phi}}{\partial \phi^2}+D_{efm,z}\frac{\partial^2 C_{s,z}}{\partial z^2}=r_A$$

$$\lambda_{s,r}\left(\frac{\partial^2 T_{s,r}}{\partial r^2}+\frac{1}{r}\frac{\partial T_{s,r}}{\partial r}\right)+\lambda_{s,\phi}\frac{1}{r^2}\frac{\partial^2 T_{s,\phi}}{\partial \phi^2}+\lambda_{s,z}\frac{\partial^2 T_{s,z}}{\partial z^2}=r_A.\Delta H_{Rx}$$

Fluid Phase:

$$\left[u_r\frac{\partial C_{A,r}}{\partial r}+u_\phi\frac{1}{r}\frac{\partial C_{A,\phi}}{\partial \phi}+u_z\frac{\partial C_{A,z}}{\partial z}\right]=k_m\left(C_A-C_s\right)$$

$$\left[u_r\rho c_p\frac{\partial T_{f,r}}{\partial r}+u_\phi\rho c_p\frac{1}{r}\frac{\partial T_{f,\phi}}{\partial \phi}+u_z\rho c_p\frac{\partial T_{f,z}}{\partial z}\right]=h_{fs}\left(T_w-T_s\right)$$

Boundary Conditions:

Inside Particle interface

$$\left[D_{efm,r}\frac{\partial C_{s,r}}{\partial r}+D_{efm,\phi}\frac{1}{r}\frac{\partial C_{s,\phi}}{\partial \phi}+D_{efm,z}\frac{\partial C_{s,z}}{\partial z}\right]=k_m\left(C_A-C_s\right)$$

$$\left[\lambda_{s,r}\frac{\partial T_{f,r}}{\partial r}+\lambda_{s,\phi}\frac{1}{r}\frac{\partial T_{f,\phi}}{\partial \phi}+\lambda_{s,z}\frac{\partial T_{f,z}}{\partial z}\right]=h_{fs}\left(T_w-T_s\right)$$

Wall Temperature Flux

$$\left[\lambda_{f,r}\frac{\partial T_{f,r}}{\partial r}+\lambda_{f,\phi}\frac{1}{r}\frac{\partial T_{f,\phi}}{\partial \phi}+\lambda_{f,z}\frac{\partial T_{f,z}}{\partial z}\right]=h_w\left(T_f-T_w\right)$$

No flux at tube wall

$$\left[\frac{\partial C_{A,r}}{\partial r}+\frac{1}{r}\frac{\partial C_{A,\phi}}{\partial \phi}+\frac{\partial C_{A,z}}{\partial z}\right]=0$$

Navier Stokes Porous media:

$$r:\frac{\rho}{\varepsilon_p}\left(\frac{u_r}{\varepsilon_p}\frac{\partial u_r}{\partial r}+\frac{u_\phi}{\varepsilon_p r}\frac{\partial u_r}{\partial \phi}+\frac{u_z}{\varepsilon_p}\frac{\partial u_r}{\partial z}-\frac{u_\phi^2}{r}\right)=-\frac{\partial p}{\partial r}+\frac{\mu}{\varepsilon_p}\left[\frac{1}{r}\frac{\partial}{\partial r}\left(r\frac{\partial u_r}{\partial r}\right)+\frac{1}{r^2}\frac{\partial^2 u_r}{\partial \phi^2}+\frac{\partial^2 u_r}{\partial z^2}-\frac{u_r}{r^2}-\frac{2}{r^2}\frac{\partial u_\phi}{\partial \phi}\right]+\frac{2\mu}{3\varepsilon_p}\left[\frac{1}{r}\frac{\partial}{\partial r}\left(r\frac{\partial u_r}{\partial r}\right)+\frac{1}{r^2}\frac{\partial^2 u_r}{\partial \phi^2}+\frac{\partial^2 u_r}{\partial z^2}-\frac{u_r}{r^2}-\frac{2}{r^2}\frac{\partial u_\phi}{\partial \phi}\right]-\frac{\mu}{K_{br}}u_r$$

$$\phi:\frac{\rho}{\varepsilon_p}\left(\frac{u_r}{\varepsilon_p}\frac{\partial u_\phi}{\partial r}+\frac{u_\phi}{\varepsilon_p r}\frac{\partial u_\phi}{\partial \phi}+\frac{u_z}{\varepsilon_p}\frac{\partial u_\phi}{\partial z}+\frac{u_r u_\phi}{r}\right)=-\frac{1}{r}\frac{\partial p}{\partial \phi}+\frac{\mu}{\varepsilon_p}\left[\frac{1}{r}\frac{\partial}{\partial r}\left(r\frac{\partial u_\phi}{\partial r}\right)+\frac{1}{r^2}\frac{\partial^2 u_\phi}{\partial \phi^2}+\frac{\partial^2 u_\phi}{\partial z^2}-\frac{u_\phi}{r^2}-\frac{2}{r^2}\frac{\partial u_\phi}{\partial \phi}\right]+\frac{2\mu}{3\varepsilon_p}\left[\frac{1}{r}\frac{\partial}{\partial r}\left(r\frac{\partial u_\phi}{\partial r}\right)+\frac{1}{r^2}\frac{\partial^2 u_\phi}{\partial \phi^2}+\frac{\partial^2 u_\phi}{\partial z^2}-\frac{u_\phi}{r^2}-\frac{2}{r^2}\frac{\partial u_\phi}{\partial \phi}\right]-\frac{\mu}{K_{br}}u_\phi$$

$$z:\frac{\rho}{\varepsilon_p}\left(\frac{u_r}{\varepsilon_p}\frac{\partial u_z}{\partial r}+\frac{u_\phi}{\varepsilon_p r}\frac{\partial u_z}{\partial \phi}+\frac{u_z}{\varepsilon_p}\frac{\partial u_z}{\partial z}\right)=-\frac{\partial p}{\partial z}+\frac{\mu}{\varepsilon_p}\left[\frac{1}{r}\frac{\partial}{\partial r}\left(r\frac{\partial u_z}{\partial r}\right)+\frac{1}{r^2}\frac{\partial^2 u_z}{\partial \phi^2}+\frac{\partial^2 u_z}{\partial z^2}\right]+\frac{2\mu}{3\varepsilon_p}\left[\frac{1}{r}\frac{\partial}{\partial r}\left(r\frac{\partial u_z}{\partial r}\right)+\frac{1}{r^2}\frac{\partial^2 u_z}{\partial \phi^2}+\frac{\partial^2 u_z}{\partial z^2}\right]-\frac{\mu}{K_{br}}u_z$$

Continuity equation:

$$\frac{1}{r}\frac{\partial\left(\rho r u_r\right)}{\partial r}+\frac{1}{r}\frac{\partial\left(\rho u_\phi\right)}{\partial \phi}+\frac{\partial\left(\rho u_z\right)}{\partial z}=0$$

G. Appendix G: Fixed Bed Reactor Data

G1: Fixed Bed Experimental Data

Metal species content in condensed sulphuric acid:

Analysis (ICP-AES) was conducted on a sample of sulphuric acid to determine the content of the acid with regard to metal sulphates formed as a result of corrosion and the dominating metal elements found in the acid mixture can be seen in Figure G-1.

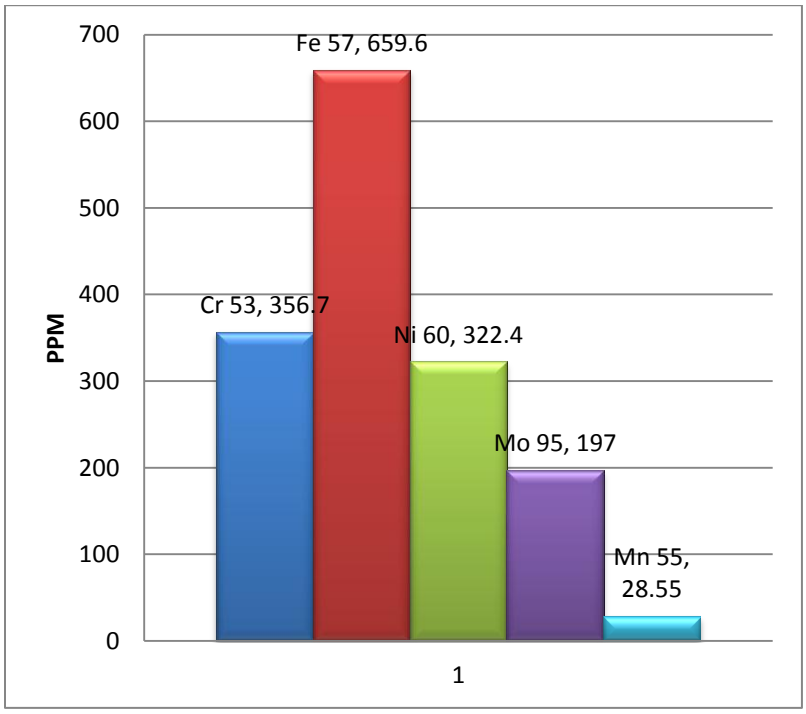

Figure G-1: Metal content in sulphuric acid solution

The high corrosivity of sulphuric acid causes high rate of corrosion in stainless steel by leaching metal ions and forming metal-sulphate combinations. The data in Figure G-1 were found from an acid sample where the whole reactor system was constructed of SS316L. The acid sample collected had a green colour and as found from analysis there was a high concentration of metal ions in the solution. This is just to verify that the amount of acid condensed will not necessarily be 100% of the theoretical amount since the Hastelloy c-276 reactor was also equipped with some stainless steel fittings.

G2: Heterogeneous Model Data

G.2.1 Model properties

The values used in the 2D homogeneous and heterogeneous model are given in Table G-1. Due to the large quantity of data collected only one set of model data is given in the table.

Table G-1: Model properties of 2D homo and heterogeneous models

	Fluid			Solid	
Parameter	**903**	**Units**	**Parameter**	**903**	**Units**
Concentration					
ε_f	0.36	-	ε_p	0.16	-
ρ_b	1177	kg/m^3	ρ_b	2443	Kg/m^3
D_m	3.5x10^{-5}	m^2/s	D_{efs}	4.2x10^{-6}	m^2/s
C_{a0}	3.19	mol/m^3	D_k	9.5x10^{-6}	m^2/s
C_{b0}	0.56	mol/m^3	$D_{eff,m}$	1.43x10^{-7}	m^2/s
C_{c0}	0.28	mol/m^3	τ	1.43	-
C_{i0}	4.19	mol/m^3			
C_{n0}	5.67	mol/m^3			
Thermal					
λ_f	0.055	W/m.K	λ_s	3.5	W/m.K
$\bar{M}_w$	0.0273	kg/mol	$c_{p,s}$	935	J/kg.K
$c_{p,f}$	52	J/mol.K	$T_{s,0}$	903	K

T_0	903	K			
P_0	105	kPa			
ε_f	0.36	-			
ρ_f	0.49	kg/m^3			
μ_f	3x10^{-5}	Pa.s			

G.2.2 Supplementary data

Table G-2 provides the error percentage for the average conversion predicted by the advance model versus experimental results obtained.

Table G-2: Error percentages for average conversion by model versus experimental

	Temperature (K)			
Velocity	**903**	**953**	**1003**	**1053**
1 m/s	14	16	11	10
1.23 m/s	16	11	15	53
1.32 m/s	8	1	12	31

H. Appendix H: Catalyst Characteristics

H1: H_2 Chemisorption:

Sample 1

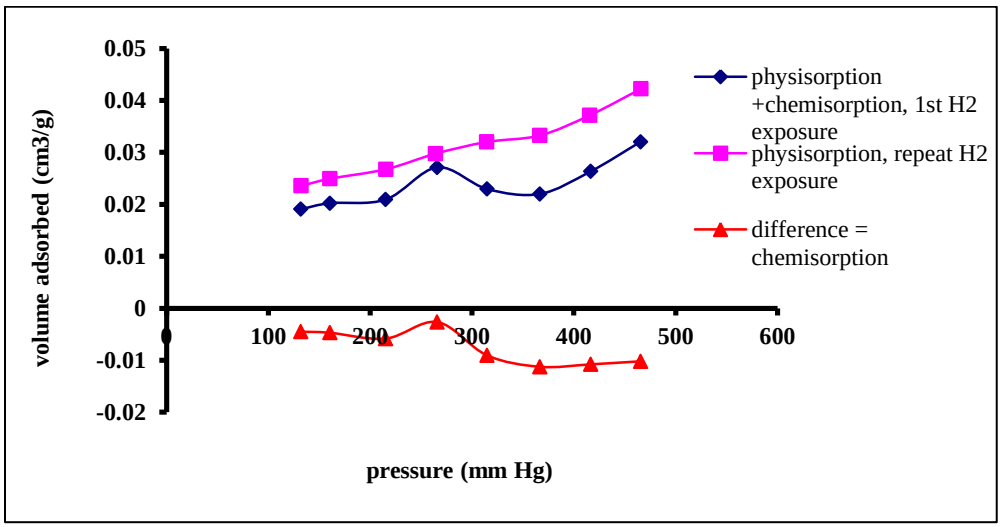

Figure H-1: H_2 Chemisorption – Sample 1

Sample 2:

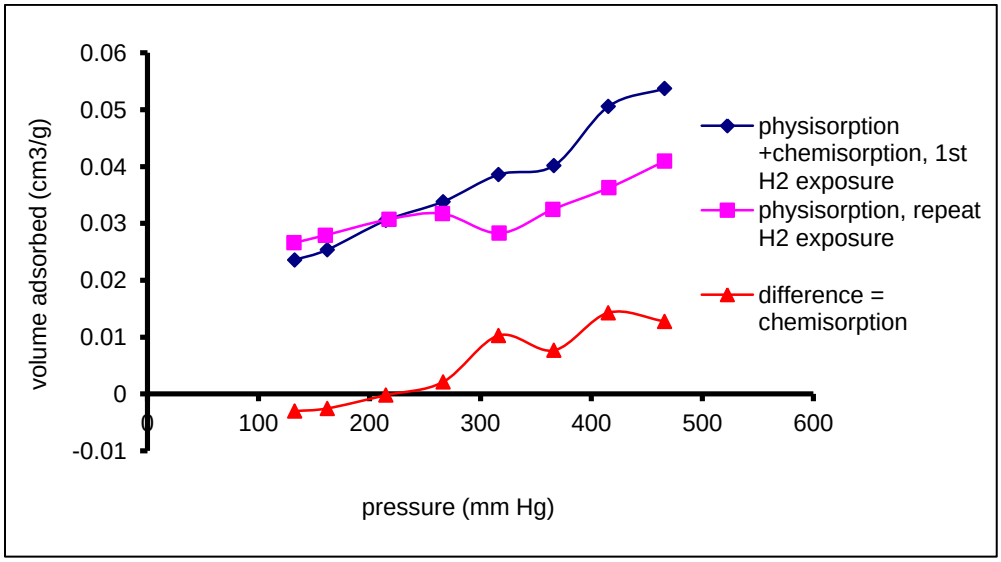

Figure H-2: H_2 Chemisorption – Sample 2

Sample 3:

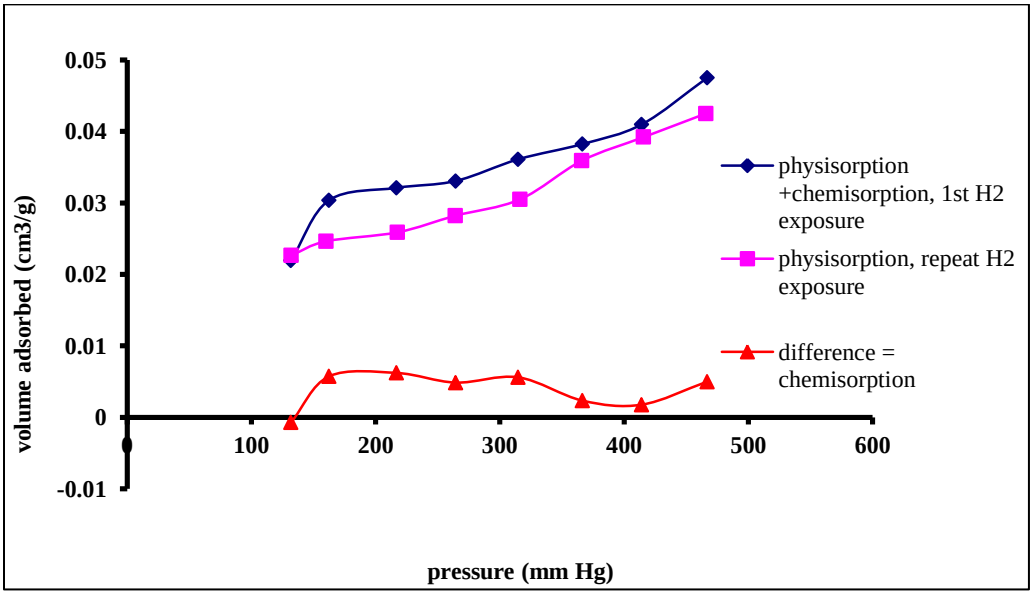

Figure H-3: H_2 Chemisorption – Sample 3

Sample 4:

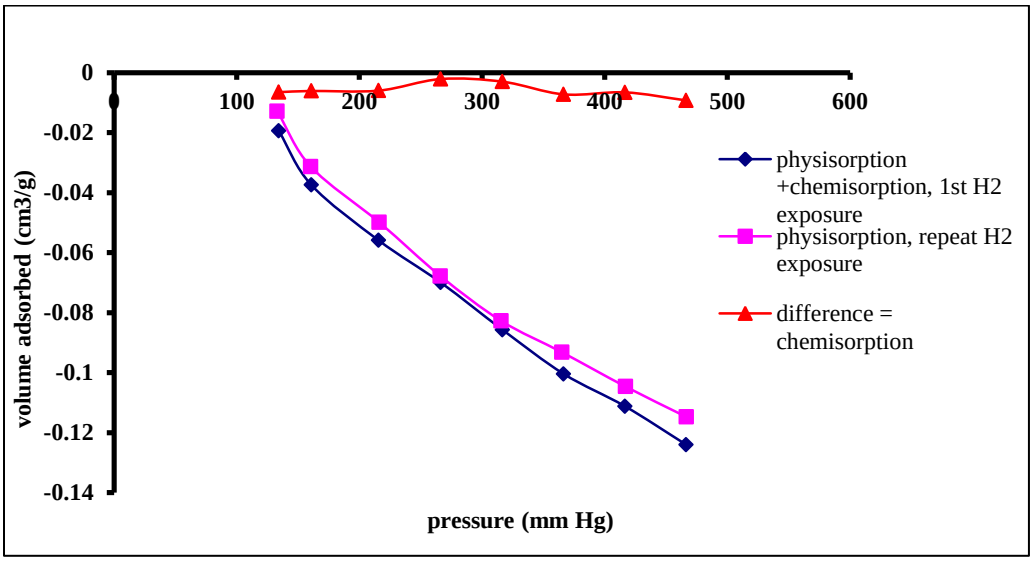

Figure H-4: H_2 Chemisorption – Sample 4

Sample 5:

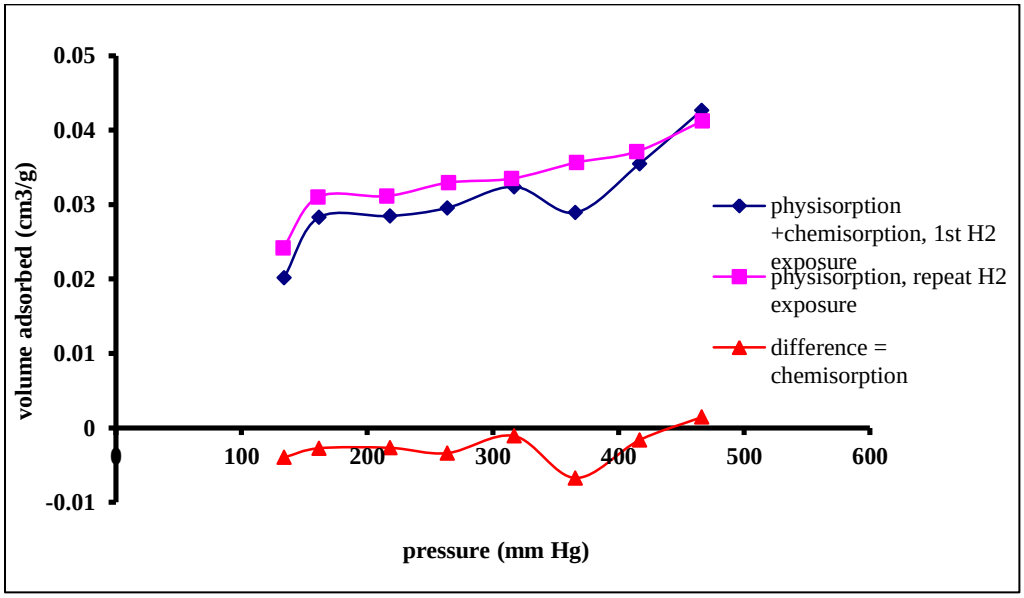

Figure H-5: H_2 Chemisorption – Sample 5

Sample 6:

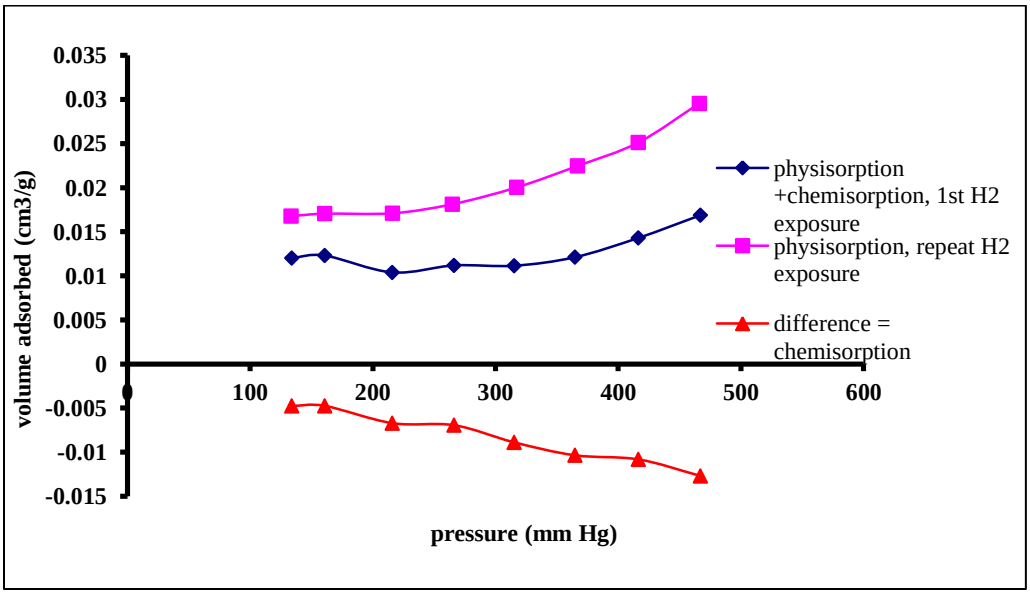

Figure H-6: H_2 Chemisorption – Sample 6

Table H-1: H_2 Chemisorption analysis results (Sample numbers indicated)

	1	2	3	4	5	6
Metal Dispersion:	2.6634 %	1.8451 %	2.9850 %	2.3120 %	2.9252 %	1.5623 %
Metallic Surface Area (m^2/g sample):	0.0658	0.0456	0.0737	0.0571	0.0722	0.0386
Metallic Surface Area (m^2/g metal):	6.5782	4.5571	7.3725	5.7103	7.2247	3.8586
Crystallite Size (6.000 V / A) (nm):	42.52223	61.38109	37.94099	48.98497	38.71696	72.49229
Y-Intercept Quantity Adsorbed (cm^3/g STP):	0.0153 ± 0.0027	0.0106 ± 0.0019	0.0171 ± 0.0023	0.0133 ± 0.0045	0.0168 ± 0.0033	0.0090 ± 0.0016
Slope:	0.000029 ± 0.000009	0.000090 ± 0.000006	0.000061 ± 0.000007	-0.000303 ± 0.000014	0.000048 ± 0.000011	0.000012 ± 0.000005
Correlation Coefficient:	8.06510E-01	9.86979E-01	9.60302E-01	-9.93311E-01	8.77398E-01	6.96960E-01
Difference Results						
Metal Dispersion:	-0.1300 %	-1.9145 %	0.5910 %	-0.6817 %	-0.8698 %	-0.2054 %
Metallic Surface Area (m^2/g sample):	-0.0032	-0.0473	0.0146	-0.0168	-0.0215	-0.0051
Metallic Surface Area (m^2/g metal):	-0.3210	-4.7284	1.4596	-1.6837	-2.1483	-0.5073
Crystallite Size (6.000 V / A) (nm):	-871.37927	-59.15695	191.64297	-166.13772	-130.20372	-551.38294
Y-Intercept Quantity	-0.0007 ±	-0.0110 ±	0.0034 ±	-0.0039 ±	-0.0050 ±	-0.0012 ±

Adsorbed (cm^3/g STP):	0.0020	0.0022	0.0026	0.0023	0.0023	0.0004
Slope:	-0.000023 ± 0.000006	0.000055 ± 0.000007	0.000002 ± 0.000008	-0.000007 ± 0.000007	0.000008 ± 0.000007	-0.000024 ± 0.000001
Correlation Coefficient:	-8.19069E-01	9.53219E-01	7.62321E-02	-3.45515E-01	4.14597E-01	-9.90468E-01

H2: N_2 Physisorption (BET)

Sample 1:

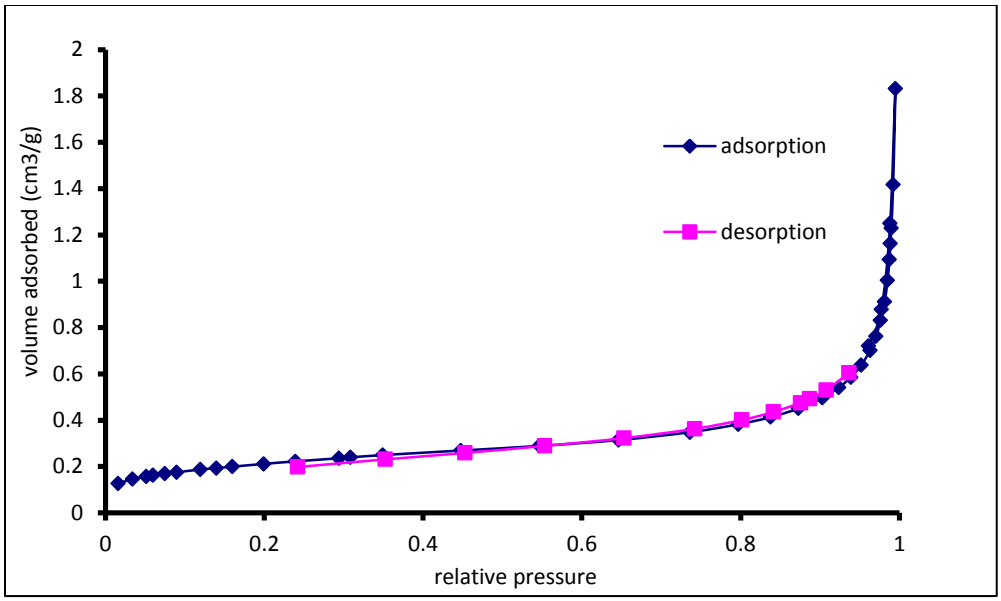

Figure H-7: BET Analysis – Sample 1

Sample 2:

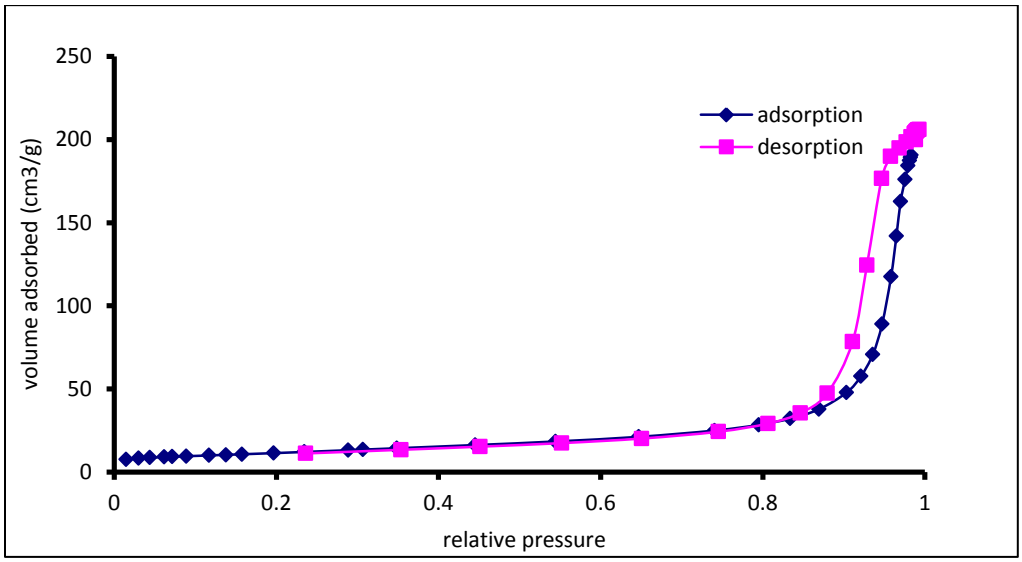

Figure H-8: BET Analysis – Sample 2

Sample 3:

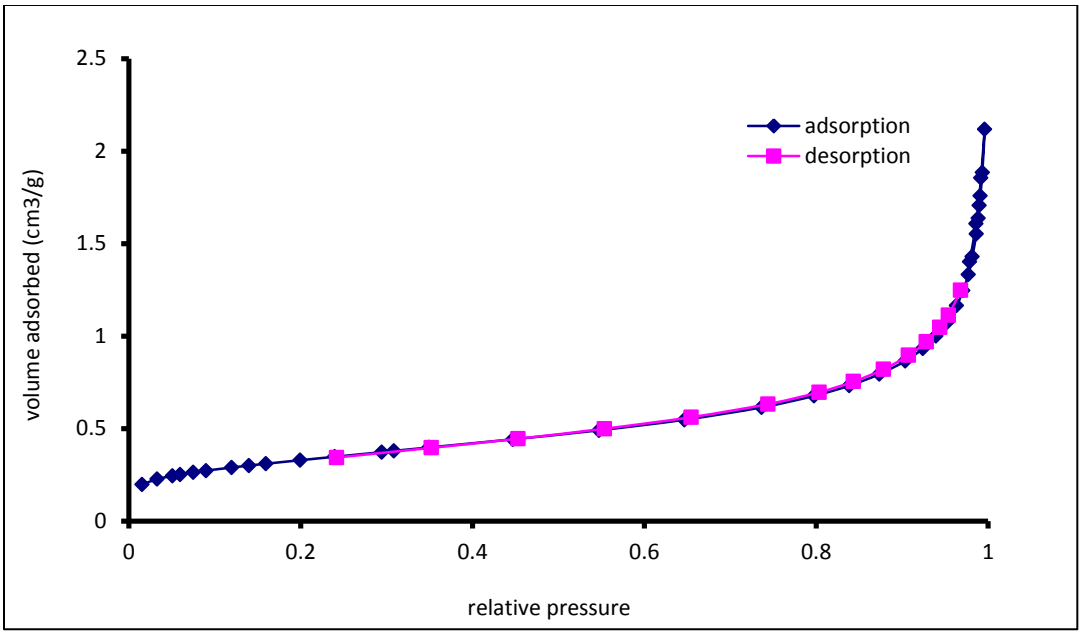

Figure H-9: BET Analysis – Sample 3

Sample 4:

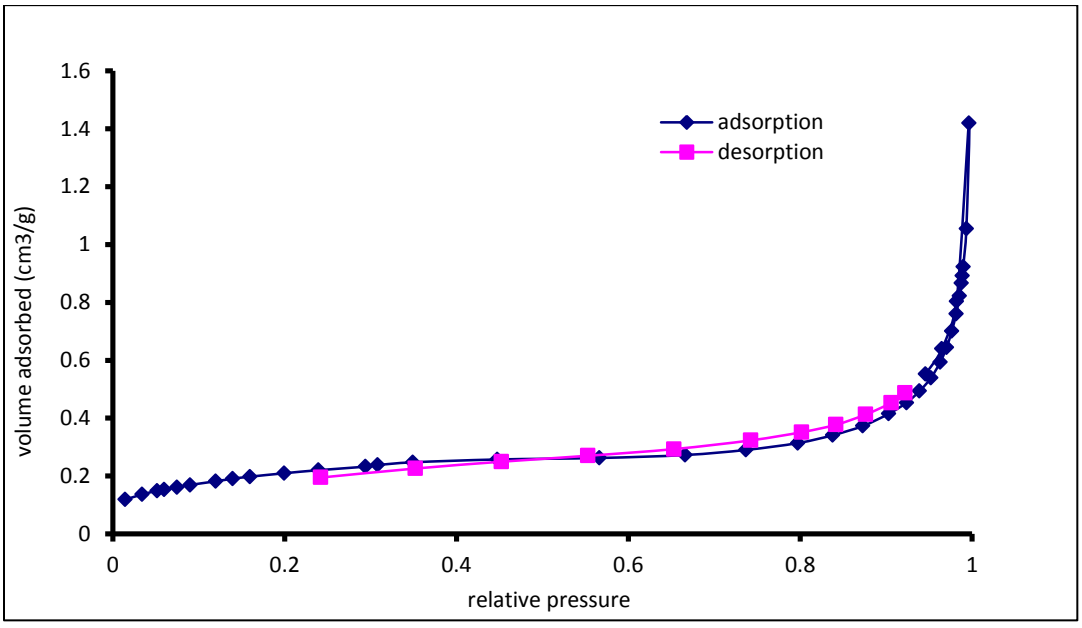

Figure H-10: BET Analysis – Sample 4

Sample 5:

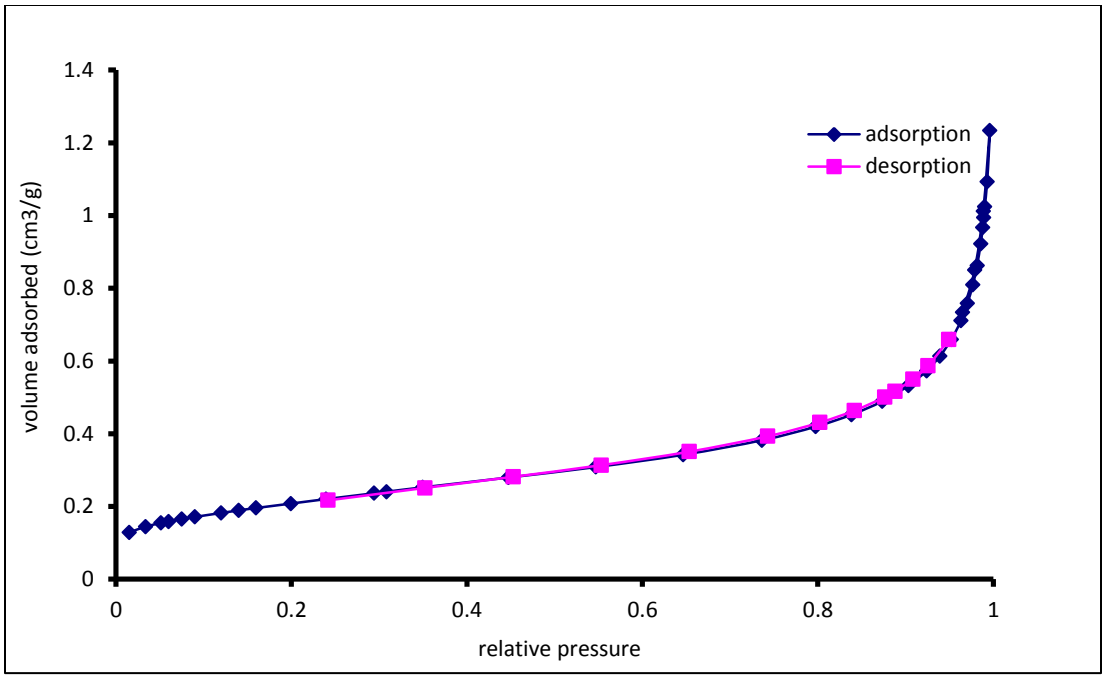

Figure H-11: BET Analysis – Sample 5

Sample 6:

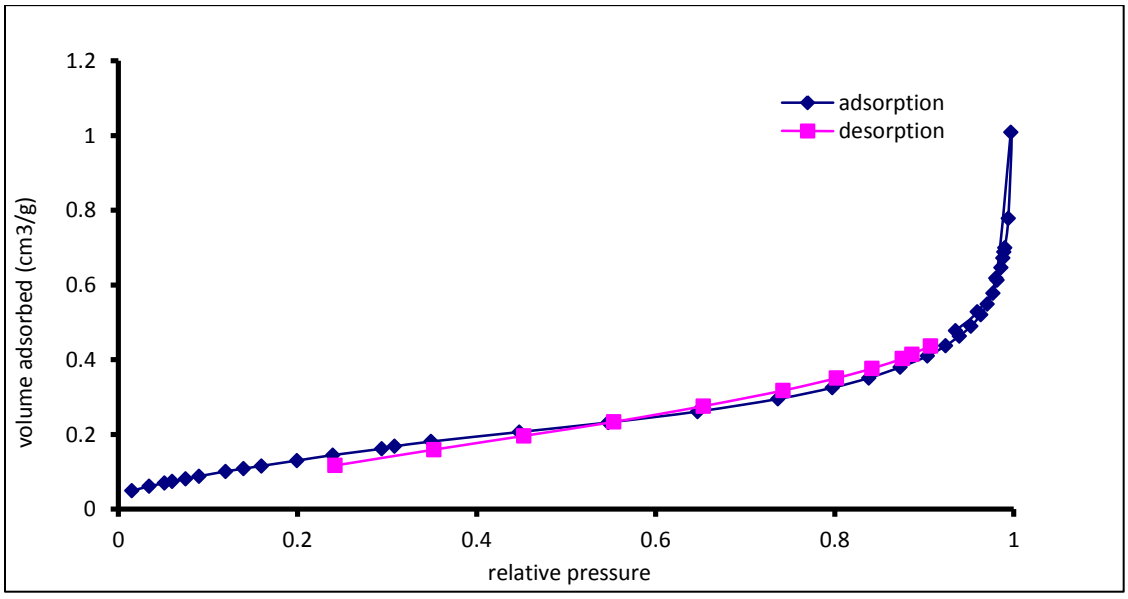

Figure H-12: BET Analysis – Sample 6

H3: TPR Analysis

Sample 1:

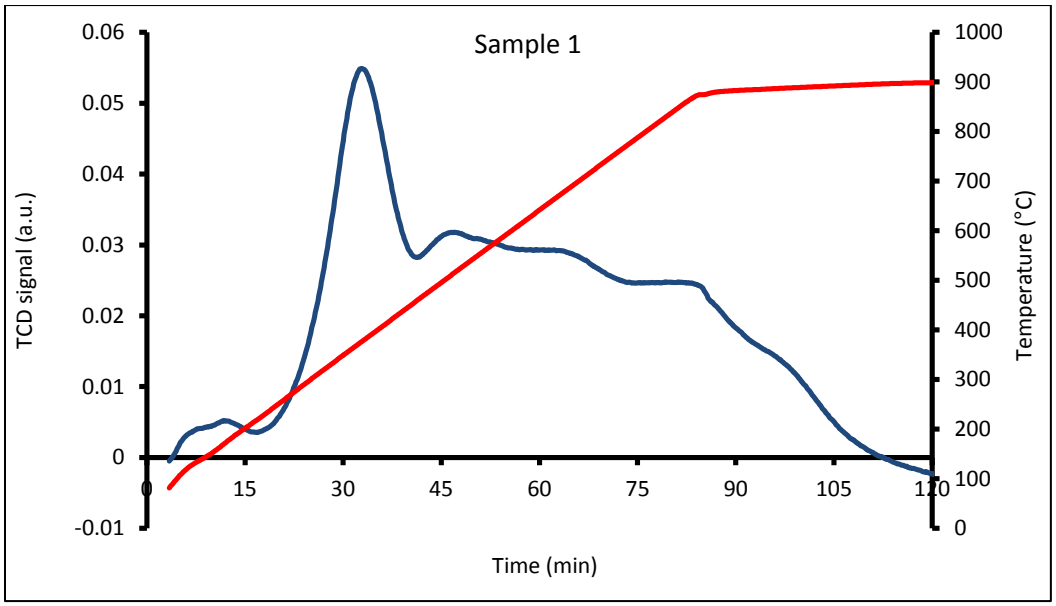

Figure H-13: TPR Analysis – Sample 1

Sample 2:

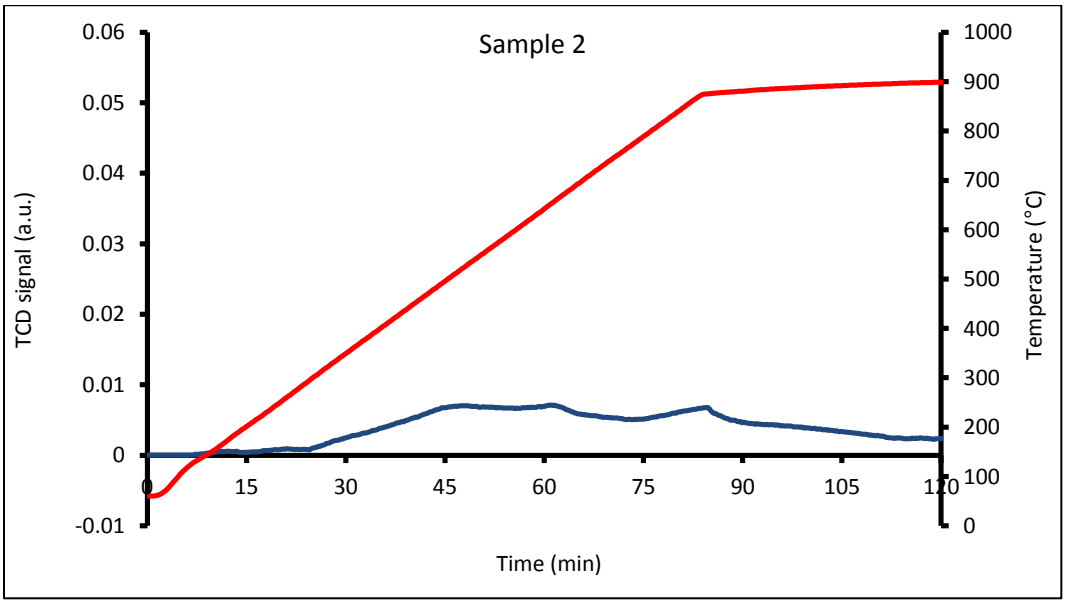

Figure H-14: TPR Analysis – Sample 2

Sample 3:

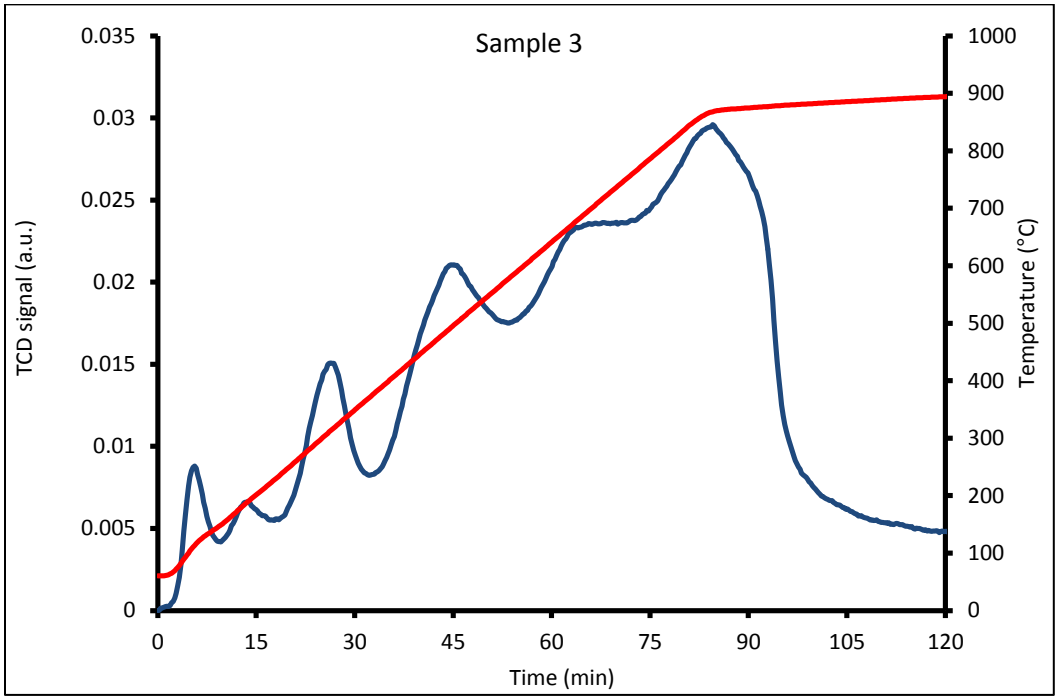

Figure H-15: TPR Analysis – Sample 3

Sample 4:

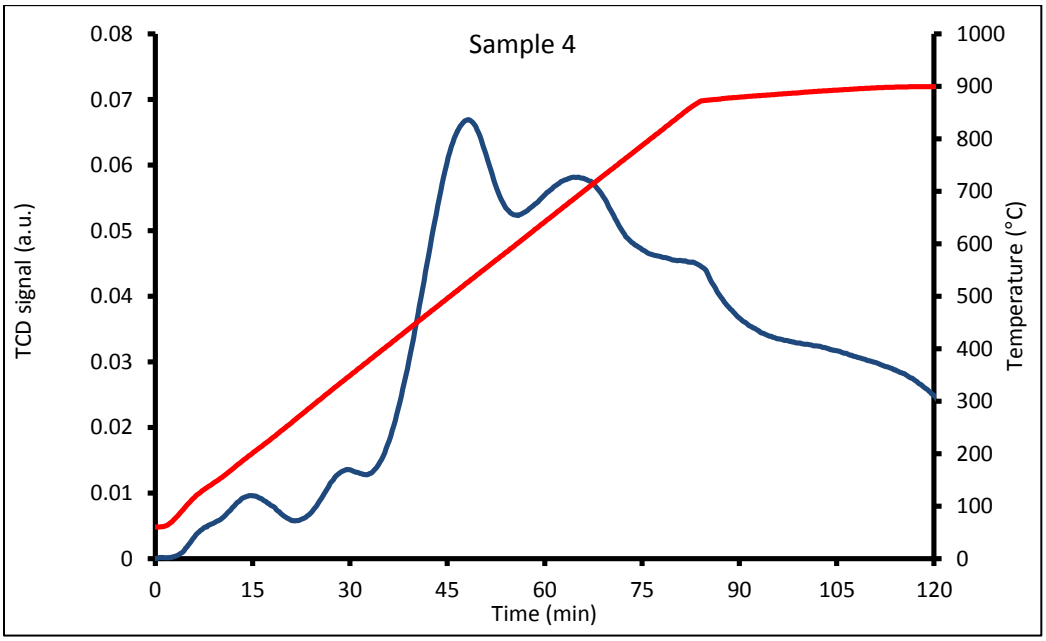

Figure H-16: TPR Analysis – Sample 4

Sample 5:

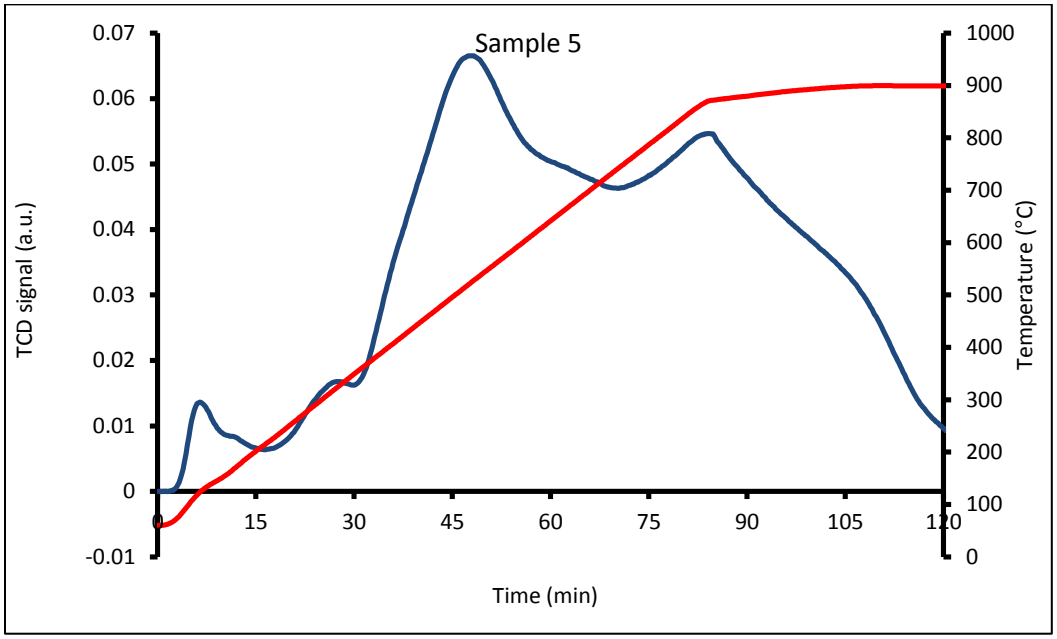

Figure H-17: TPR Analysis – Sample 5

Sample 6:

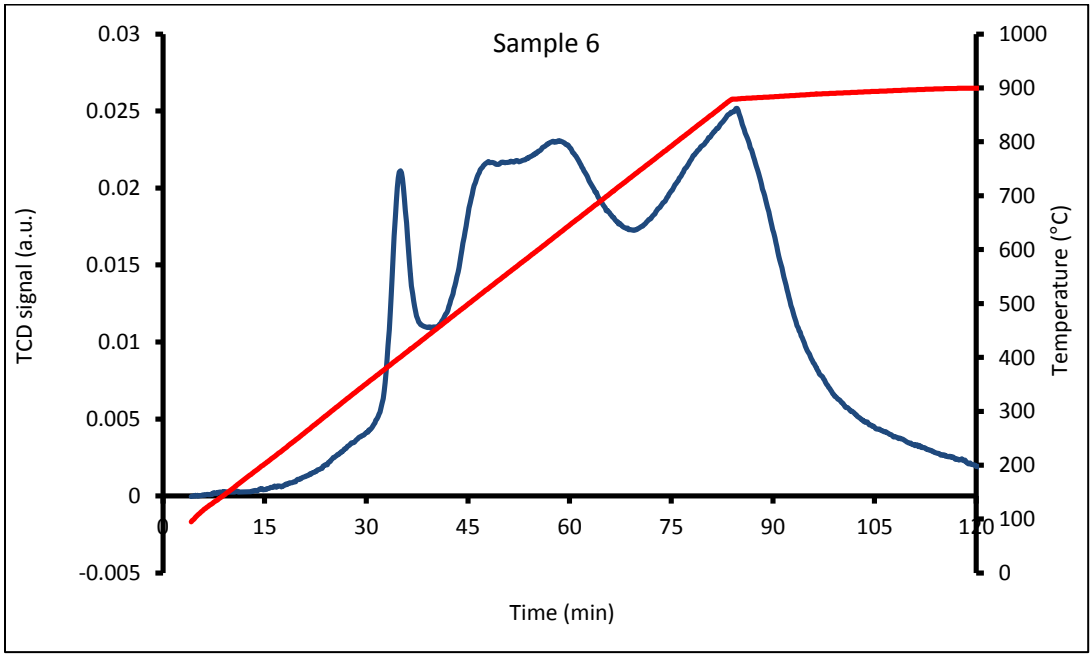

Figure H-18: TPR Analysis – Sample 6

H4: TEM Images

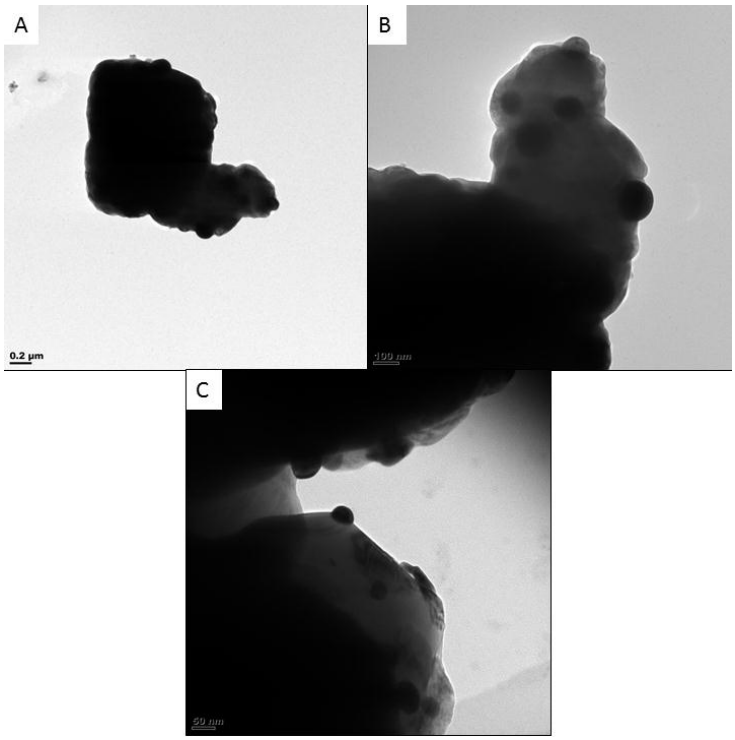

Figure H-19: TEM Images of Sample 1; A: 0.2 µm; B: 100 nm; C: 50 nm

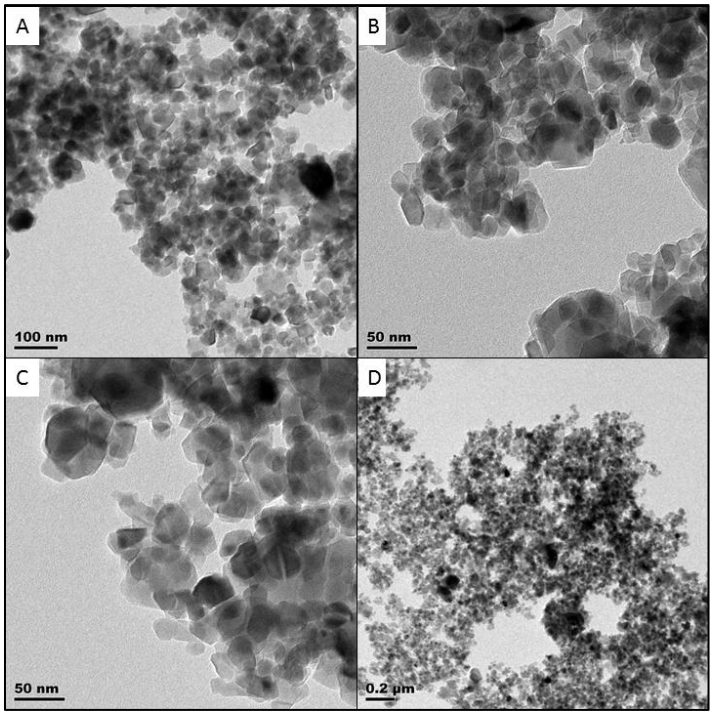

Figure H-20: TEM Images of Sample 2: A: 100 nm; B: 50 nm; C: 50 nm; D: 0.2 µm

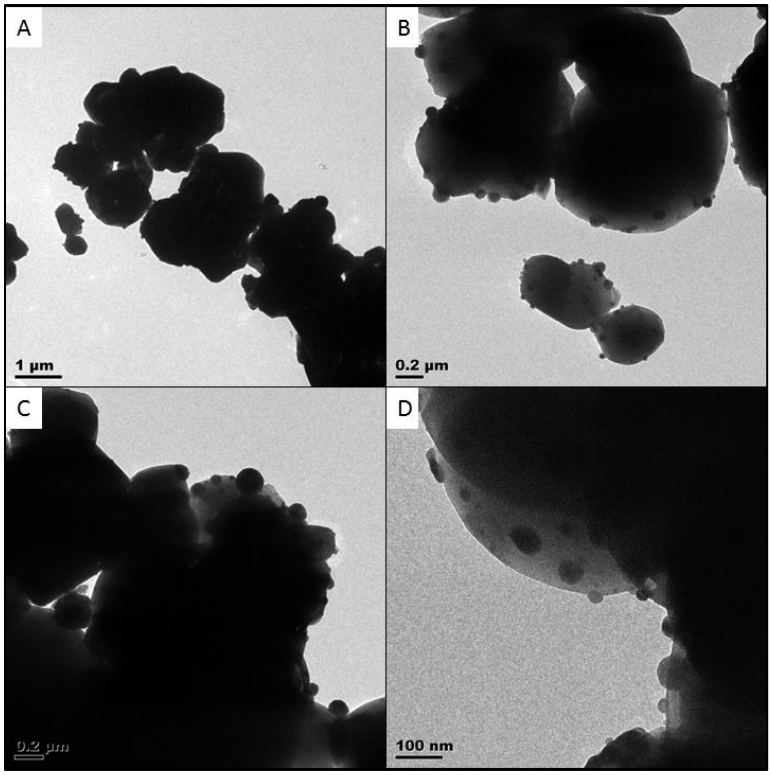

Figure H-21: TEM Images of Sample 3; A: 1 µm; B: 0.2 µm; C: 0.2 µm; D: 100 nm

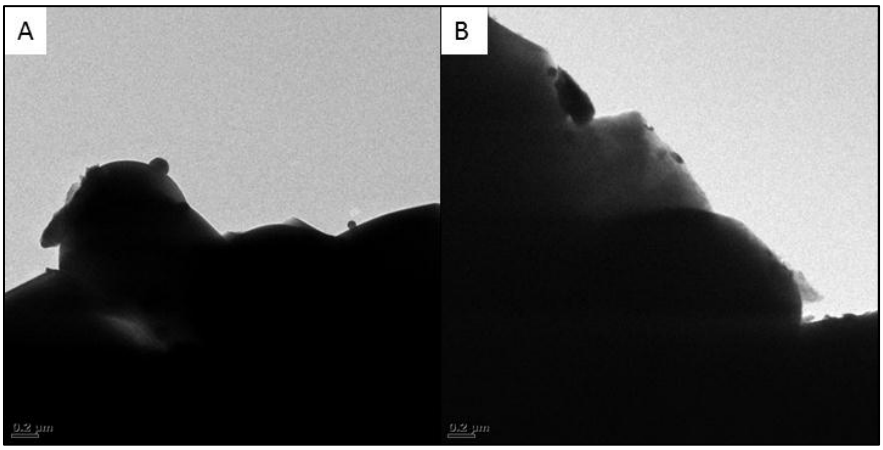

Figure H-22: TEM Images of Sample 4; A: 0.2 µm; B: 0.2 µm

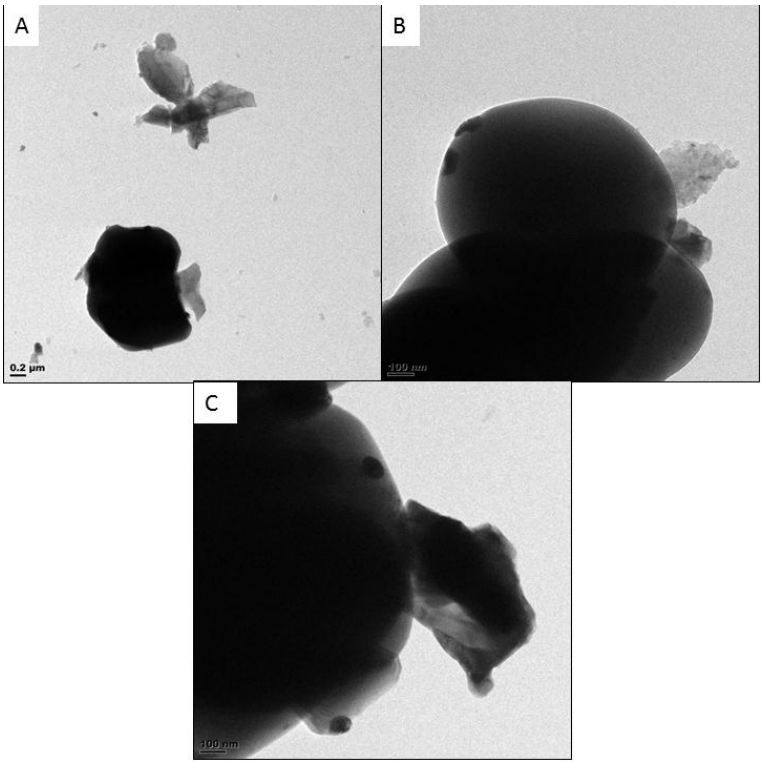

Figure H-23: TEM Images of Sample 5; A: 0.2 µm; B: 100 nm; C: 100 nm

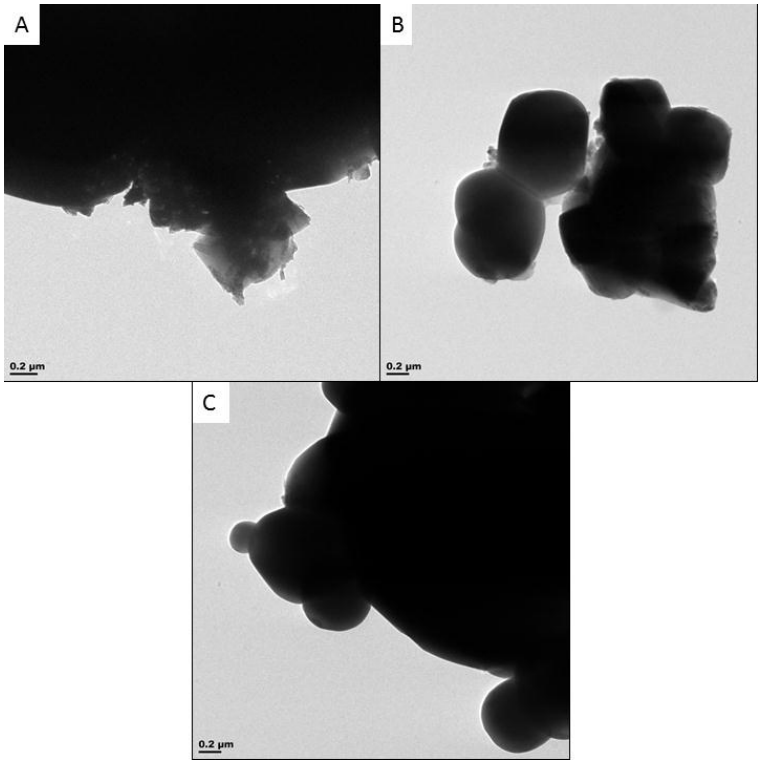

Figure H-24: TEM Images of Sample 6: A: 0.2 µm; B: 0.2 µm; C: 0.2 µm

H5: XRD Results

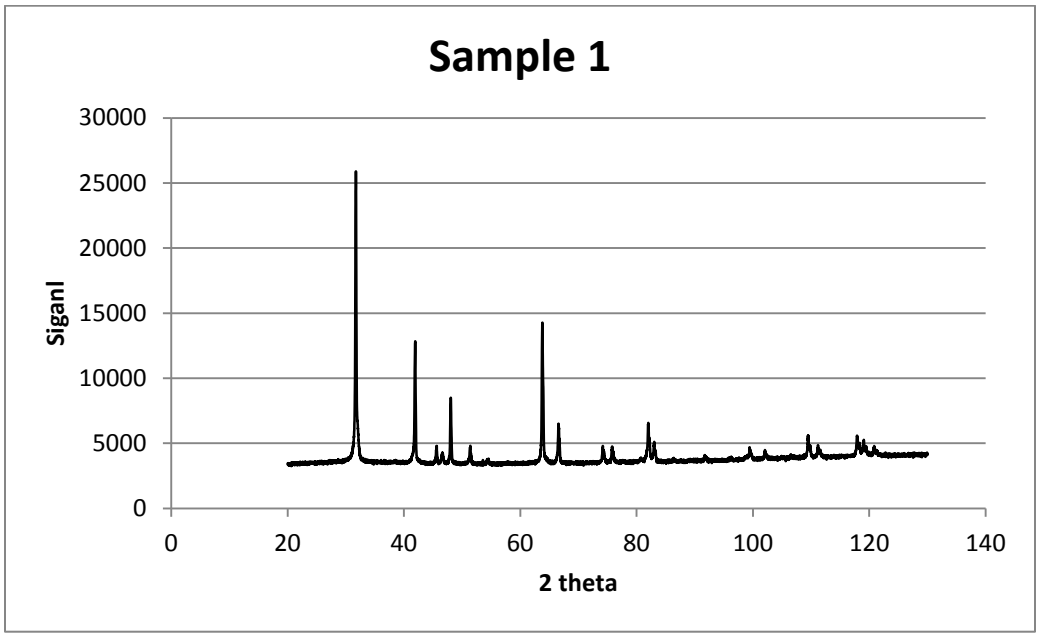

Figure H-25: X-Ray Diffraction Spectrum Sample 1

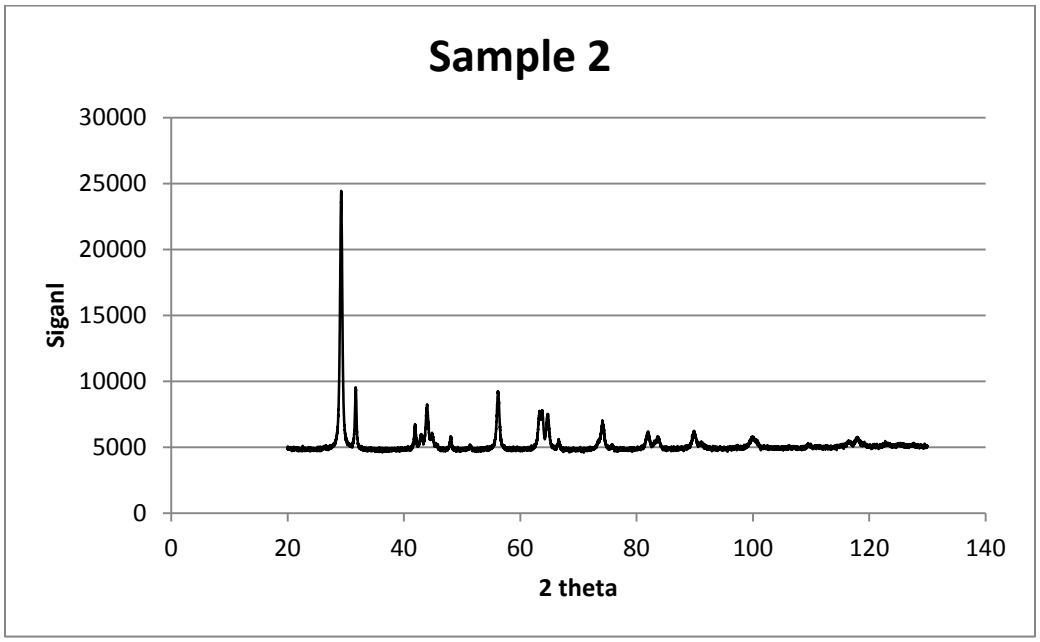

Figure H-26: X-Ray Diffraction Spectrum Sample 2

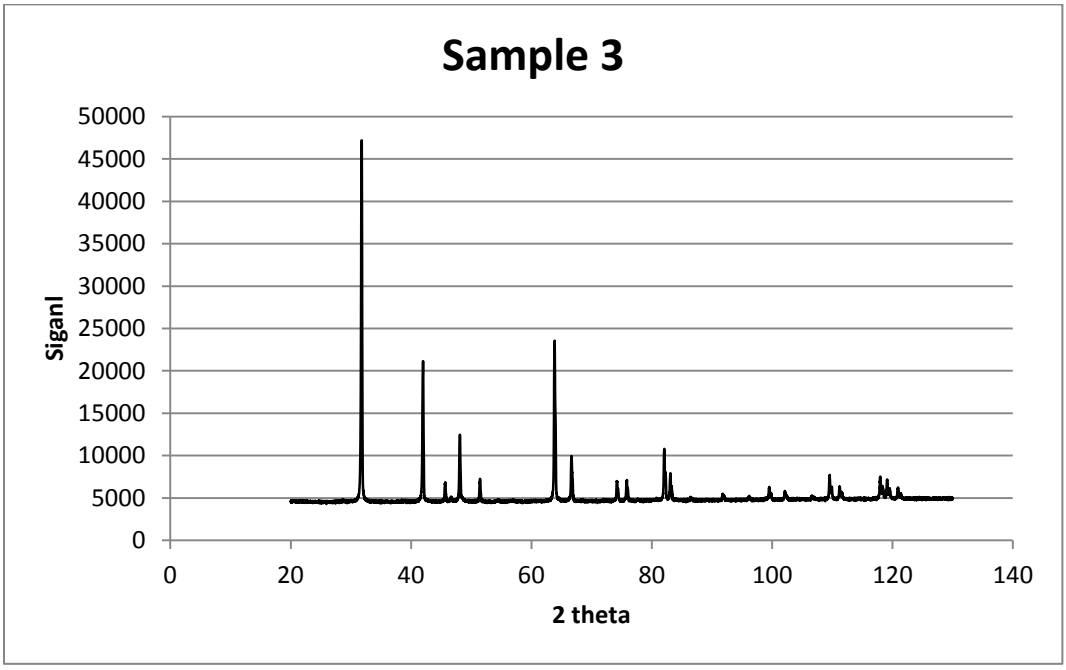

Figure H-27: X-Ray Diffraction Spectrum Sample 3

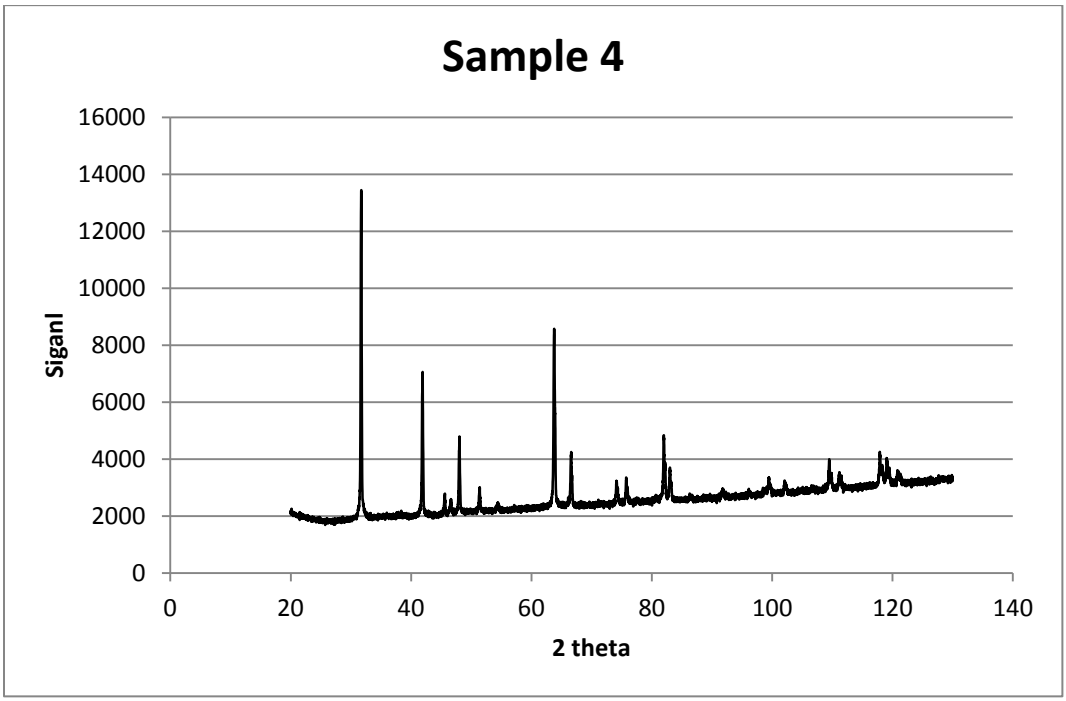

Figure H-28: X-Ray Diffraction Spectrum Sample 4

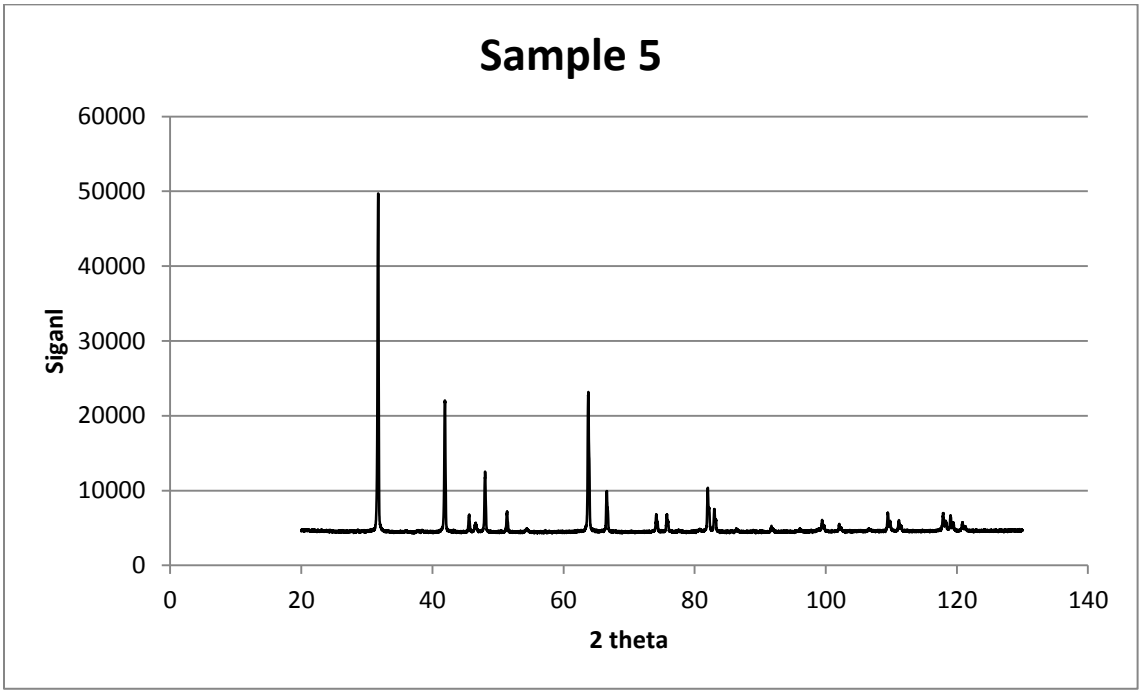

Figure H-29: X-Ray Diffraction Spectrum Sample 5

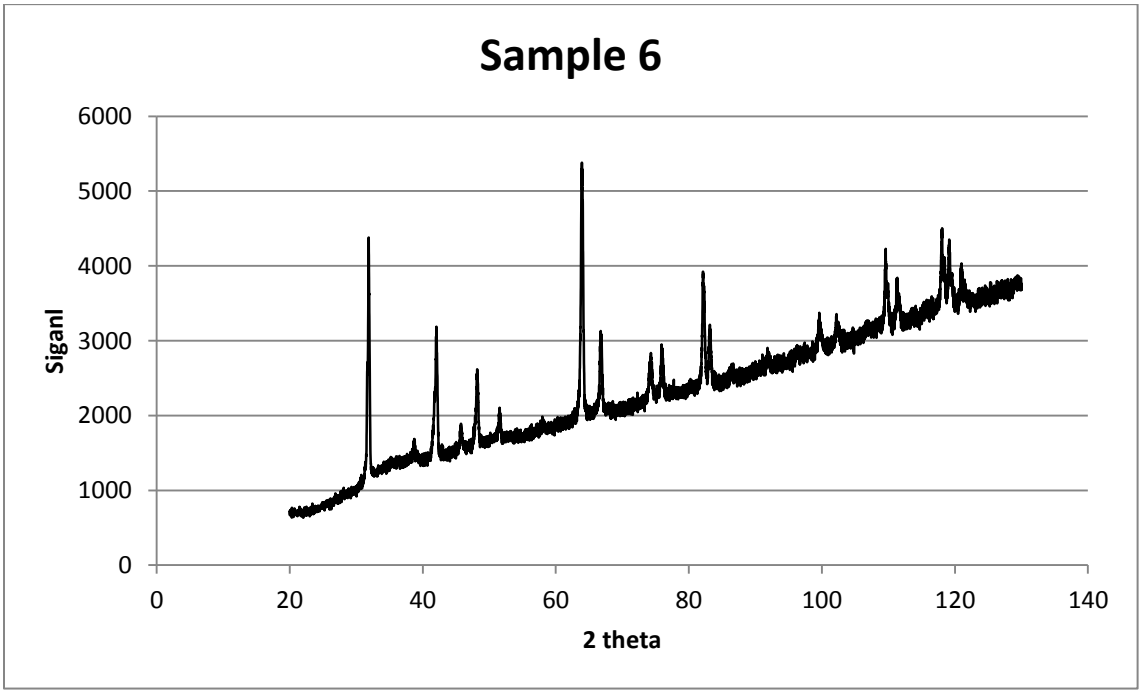

Figure H-30: X-Ray Diffraction Spectrum Sample 6